Currents and Water Masses of the Coastal Transition Zone off Northern California, June to August 1988

ADRIANA HUYER,[1] P. MICHAEL KOSRO,[1] JANE FLEISCHBEIN,[1] STEVEN R. RAMP,[2] TIM STANTON,[2] LIBE WASHBURN,[3,4] FRANCISCO P. CHAVEZ,[5] TIMOTHY J. COWLES,[1] STEPHEN D. PIERCE,[1] AND ROBERT L. SMITH[1]

In summer 1988, we made repeated mesoscale surveys of a grid extending 200 km offshore between 37°N and 39°N in the coastal transition zone off northern California, obtaining continuous acoustic Doppler current profiler data and conductivity-temperature-depth data at standard stations 25 km apart on alongshore sections 40 km apart. All surveys showed a baroclinic equatorward jet, with core velocities of >50 cm s^{-1} at the surface decreasing to about 10 cm s^{-1} at 200 m, a width of 50–75 km, and a baroclinic transport of about 4 Sv. The core of the jet lay between the 8.6 and 9.4 m^2 s^{-2} contours of geopotential anomaly (relative to 500 dbar). Three current meter moorings, deployed at 25-km separation across the jet at the beginning of the survey sequence, provided time-series of the velocity; throughout the 37-day deployment, at least one mooring was within the core defined by the 8.6 and 9.4 m^2 s^{-2} contours. The jet flowed southwestward across the grid from late June until mid-July 1988, when the jet axis moved offshore in the north and onshore in the southern portion of the grid. Temperature-salinity analysis shows that jet waters can be distinguished from both the freshly upwelled coastal waters and the offshore waters. Isopycnal maps indicate alongshore advection of relatively fresh, cool water from farther north, as well as small-scale patchiness not resolved by our survey grid. The baroclinic jet observed here may be continuous with the core of the California Current off central California. The later surveys clearly showed a poleward-flowing undercurrent adjacent to the continental slope, with core velocities up to 20 cm s^{-1} at depths of 150–250 m. Its baroclinic transport (relative to 500 dbar) increased from <0.5 Sv to >1.0 Sv between late June and early August 1988. Within the survey grid, there was a definite onshore gradient in the characteristics of North Pacific Intermediate Water. The subsurface waters adjacent to the continental margin were warmer and more saline than those offshore, indicating net northward advection by the California Undercurrent over the inshore 100 km and equatorward advection farther from shore.

INTRODUCTION

During the summer upwelling season, a complex transition zone separates the warm surface waters of the open ocean from the freshly upwelled coastal waters of northern California. Satellite images have shown tongues and filaments of cold water extending seaward across this zone [*Flament et al.*, 1985; *Zkeda and Emery*, 1984], and mesoscale surveys of the region have shown intense and narrow currents within it [*Rienecker et al.*, 1985; *Kosro and Huyer*, 1986]. The cold tongues and filaments seem to be associated with seaward-flowing "squirts" or "jets" [*Davis*, 1985; *Rienecker and Mooers*, 1989; *Thomson and Papadakis*, 1987]. Large-scale surveys conducted in 1987 [*Coastal Transition Zone (CTZ) Group*, 1988; *Kosro et al.*, this issue] suggest that these features are part of a meandering but continuous jet that flows generally equatorward at the core of the California Current, along the front that separates the productive, recently upwelled coastal waters from the relatively barren offshore waters [*Hood et al.*, 1990].

[1]College of Oceanography, Oregon State University, Corvallis.

[2]Department of Oceanography, Naval Postgraduate School, Monterey, California.

[3]Department of Geological Sciences, University of Southern California, Los Angeles.

[4]Now at Department of Geography, University of California, Santa Barbara.

[5]Monterey Bay Aquarium Research Institute, Pacific Grove, California.

In summer 1988 we undertook repeated surveys of a portion of the coastal transition zone in the Point Reyes–Point Arena region of northern California, a region where cold filaments and seaward jets seemed to persist or recur. Our intent was to sample with sufficient spatial resolution to define the structure, characteristics, and source waters of a jet and to repeat the sampling grid approximately once per week for 6 weeks in order to follow its evolution and provide background observations for more detailed studies of the high-velocity zone. All surveys were to measure both physical and biological fields: velocity profiles along the ship's track; temperature, salinity, fluorescence and optical transmission at closely spaced conductivity-temperature-depth (CTD) stations; nutrients and chlorophyll from rosette water samples; and underway monitoring of near-surface seawater. An array of current meters, including two upward-looking acoustic Doppler current profilers (ADCPs), was moored across the axis of the jet during the first survey and recovered at the beginning of the last survey. The chemical and biological fields are described by *Chavez et al.* [this issue] and T. J. Cowles et al. (Distribution patterns of particulate matter in a cold filament of the California Current system, submitted to *Journal of Geophysical Research*, 1991, hereinafter referred to as Cowles et al. (1991)). In this paper we describe the velocity and water property fields, using maps and cross sections to define the structure and evolution of the jet, and water mass analysis to determine its characteristics and source waters. Finally, we discuss briefly the observed change in jet position and orientation and the relation of our observations to the larger-scale California Current system.
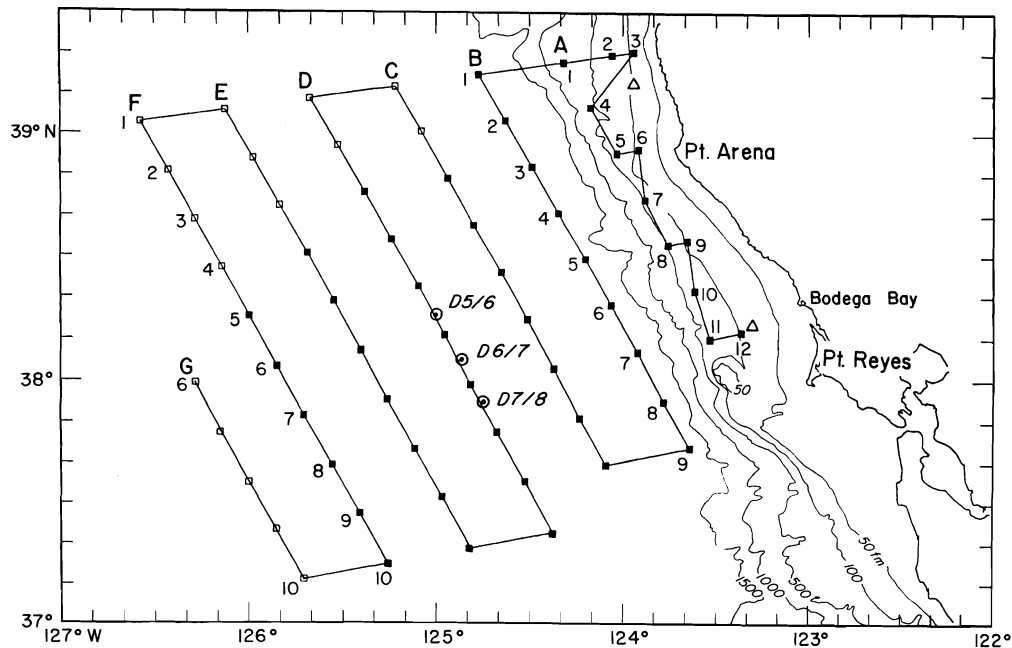
Fig. 1. The standard station grid for repeated surveys of the coastal transition zone off northern California, June–August 1988. Letters designate alongshore sections, and numbers designate station positions along each section; the sections were not always occupied in the order shown. Solid dots represent stations occupied on all five "complete" surveys. Triangles represent NDBC meteorological buoys, and circles represent current meter moorings.

OBSERVATIONS

Between mid-June and mid-August 1988 we made six repeated surveys to observe the structure and evolution of a high-velocity offshore-flowing current in the region offshore of Point Arena and Point Reyes. The standard grid (Figure 1) was designed to extend at least 200 km offshore (because features of this length had been observed earlier [*Kosro and Huyer,* 19861) and about 200 km in the alongshore direction (potentially wide enough to map the onshore return flow as well as the offshore-flowing jet [*Flament et al.,* 19851). The inshore edge of the grid lay along the upper continental slope, with a few stations over the outer shelf to define the inshore waters. Stations and sections within the grid were separated by about one internal Rossby radius of deformation (about 25 km in this region) to resolve the mesoscale spatial structure of the hydrographic fields. The overall grid size was constrained by the need to complete each survey in less than a week (prior estimates of evolution time scales were 2–3 weeks [*Rienecker et al.,* 1985]). The standard grid consisted of six sections (A to F, Figure 1) with a seventh section *(G)* added when time allowed.

The sequence of six surveys was executed jointly by investigators from several institutions using three separate ships (Table 1). The Washington survey was incomplete: ADCP current profiles were not available because of poor reception of LORAN-C navigation data, and expendable bathythermographs (XBTs) replaced CTD casts at most stations on the C and D lines because of rough weather. The other five surveys were complete, in the sense that velocity profiles were obtained along the entire ship's track, and CTD casts were made at all or most of the stations on the six standard sections (Table 1). We focus here primarily on the results of the five complete surveys.

CTD measurements on the R/V *Wecoma* and the R/V *Point Sur* were made with Neil Brown Instrument Systems

(NBIS) CTD systems, with an accuracy of about ±0.01°C in temperature and ±0.003 psu in salinity. The Sea-Bird CTD measurements from the R/V *Washington* have an accuracy of about ±0.01°C and ±0.005 psu. The XBT accuracy is about ±0.2°C. On *Wecoma* and *Point Sur,* the CTD unit was equipped with a SeaTech 25-cm transmissometer and a SeaTech fluorometer, and a 12-bottle rosette was used to

TABLE 1. Dates of the Repeated Standard-Grid Surveys, and List of Stations Occupied on Each Survey

Survey Dates	Ship	Stations Occupied
June 20–27	*Wecoma*	D1 to D10, A12 to A1, B1 to B9, C9 to C1, E3 to E10, F10 to F2, E3
June 25 to July 2	*Washington*	A13 to A1, B1 to B7, D9 to D10, E10 to E8, E6 to E3, F3 to F1O
July 6–12	*Point Sur*	A12 to A1, B1 to B9, C9 to C3, D3 to D10, E10 to E2, F4 to F10, G6 to G10
July 13–18	*Point Sur*	A12 to A1, B1 to B9, C9 to C3, D3 to D10, E10 to E4, F5 to F10, G6 to G11
July 22–26	*Point Sur*	A12 to A1, B1 to B9, C9 to C3, D3 to D10, E10 to E3, F3 to F10, G6 to G10
July 29 to August 3	*Wecoma*	A12 to A1, BO to B9, C9 to C1, D1 to D10, E10 to E1, F1 to F1O

Stations are listed in order of occupation. The standard station positions are indicated in Figure 1.
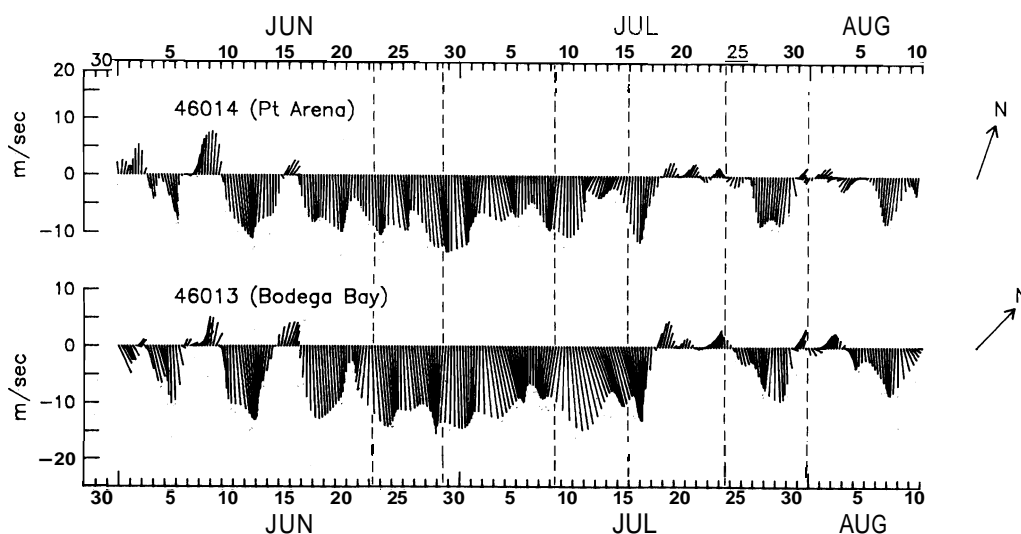
Fig. 2. Low-passed (<0.6 cpd) vector time series of the wind measured at NDBC buoys near Point Arena (relative to 341°T) and Bodega Bay (relative to 316°T). Vertical lines indicate the mid-point of each survey.

collect water samples for chlorophyll and nutrient analysis at selected standard depths; these observations are discussed by *Chavez et al.* [this issue] and by Cowles et al. (1991).

A shipborne ADCP manufactured by RD Instruments was operated continuously on the *Wecoma* and *Point Sur* cruises. Average profiles of relative velocity between the ship and the ocean were obtained about once per minute for *Wecoma* cruises and about once per 3 min for *Point Sur* cruises. On *Wecoma* a 300-kHz transducer with a nominal depth range of 240 m was used with a pulse length of 12 m (18.8 ms) and a vertical bin width of 8 m (12.6 ms). The shallowest level to yield reliable data was about 25 m. Filter skew and noise bias errors [*Chereskin et al.*, 1989] were estimated to be small (<1 cm s^{-1}) in the *Wecoma* data. On *Point Sur* a 150-kHz transducer with a nominal range of 350 m was used with a pulse length of 4 m (6.3 ms) and a bin width of 4 m (6.3 ms). For these parameters and for typical current shears, the filter skew error in the deep data can be several (0-10) centimeters per second, highest at large ship speeds and current shears [*Chereskin et al.*, 1989]. On both ships, profiles typically extended below 200 m, except when steaming into rough seas. Navigation data from a NorthStar LORAN-C receiver on each ship were recorded, edited, and combined with the relative velocity, vertically averaged across a reference layer, to calculate the ship's velocity and absolute currents. Alignment errors between the transducer and the ship's gyro compass were identified and corrected using the methods described by *Kosro* [1985]. The absolute currents were subsequently low-pass filtered to suppress signals with periods less than 30 min. In the maps presented here, the data were further averaged horizontally to 12.5-km bins (half the station separation) and vertically interpolated to 25-m depth intervals.

Upper ocean currents were also measured at three moorings near the D line (Figure 1) deployed during June 21–26 and recovered during July 27–29. One of these moorings (D6/7, midway between the D6 and D7 CTD stations) had Aanderaa current meters at depths of about 90,140,190, and 430 m. Two moorings (D5/6 and D7/8) had a self-contained 300-kHz ADCP instrument at about 116 m and Aanderaa current meters at 120, 150, 200, and 450 m. The Aanderaa

instruments recorded average speed, instantaneous direction, and temperature at 10-min intervals. The ADCPs were operated with a 6-m pulse length, 4-m bins, and a ping every 2 s; 2-min averages were recorded every 2.$ min. The ADCPs returned good quality data in 4-m bins between about 20 m and 110 m depth; data from every third bin (i.e., with 12-m separation) are completely independent. The current time-series were low-pass filtered (half-power at 35 hours) to remove tidal, inertial and high-frequency internal-wave signals.

Winds were measured once per hour at bouys maintained near the coast off Bodega Bay (buoy 46013) and Point Arena (46014) by the National Data Buoy Center (NDBC). The data were low-pass filtered (half power at 40 hours) to remove diurnal and shorter-period signals. At both locations, winds were strongly favorable for upwelling at the beginning of the survey sequence and remained so through mid-July (Figure 2).

Images of sea surface temperature from advanced very high resolution radiometer (AVHRR) sensors on NOAA 9 and NOAA 10 satellites (TIROS-N series) were collected and transformed to brightness temperature by the Scripps Satellite Facility; images were registered to Earth coordinates by M. Abbott at Oregon State University. These images show that cool tongues and filaments extending seaward from the coastal zone were present throughout the survey sequence. Many images were partly obscured by cloud cover; Figure 3 shows the best available image for each survey.

HORIZONTAL STRUCTURE OF THE TRANSITION ZONE

The Near-Surface Fields

The temporal evolution of the surface or near-surface velocity, temperature and salinity fields is shown in Figure 3 and 4. For each complete survey, Figure 3 shows the shallowest (25 m) current vectors (measured over 5–7 days by the shipborne ADCP) superimposed on an AVHRR image of the sea surface temperature. Note that the images are truly synoptic, while the surveys are only quasi-synoptic.
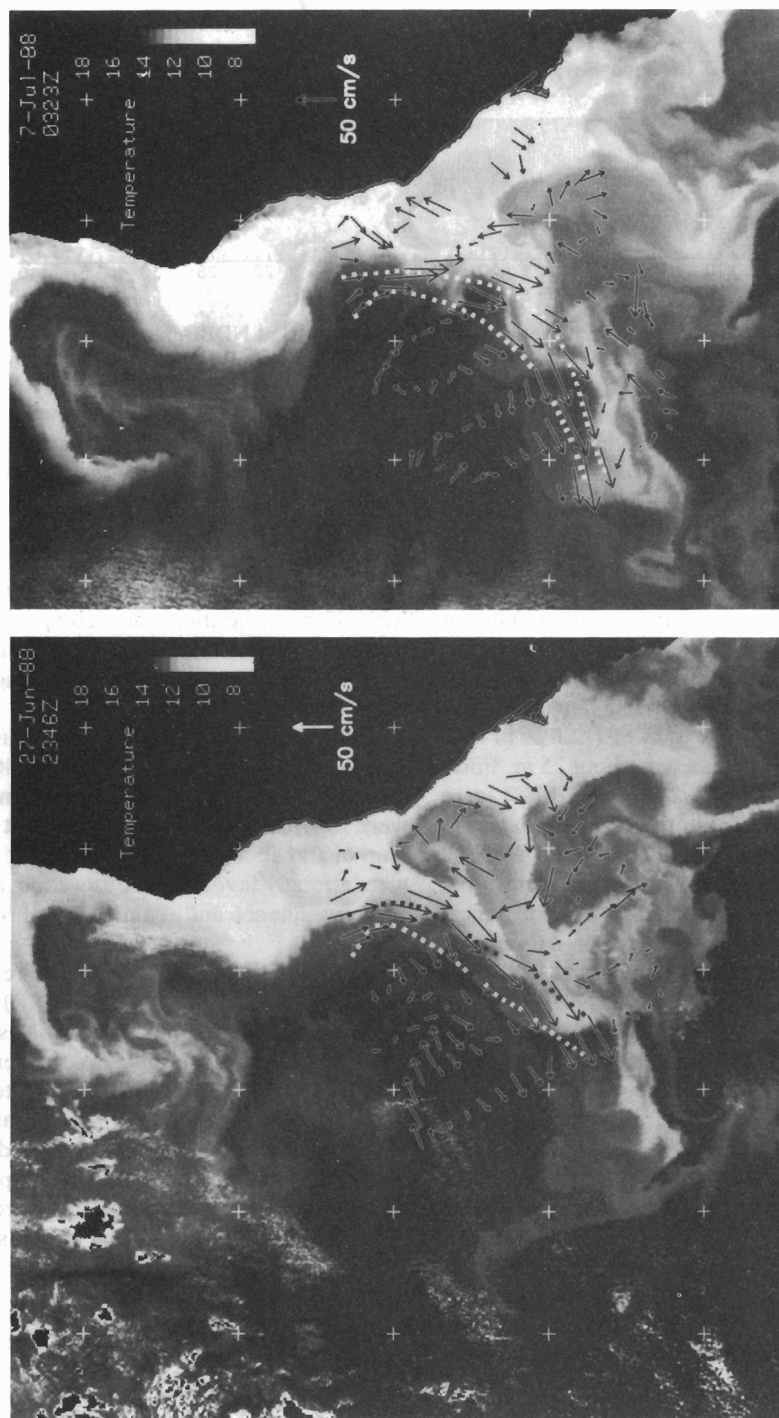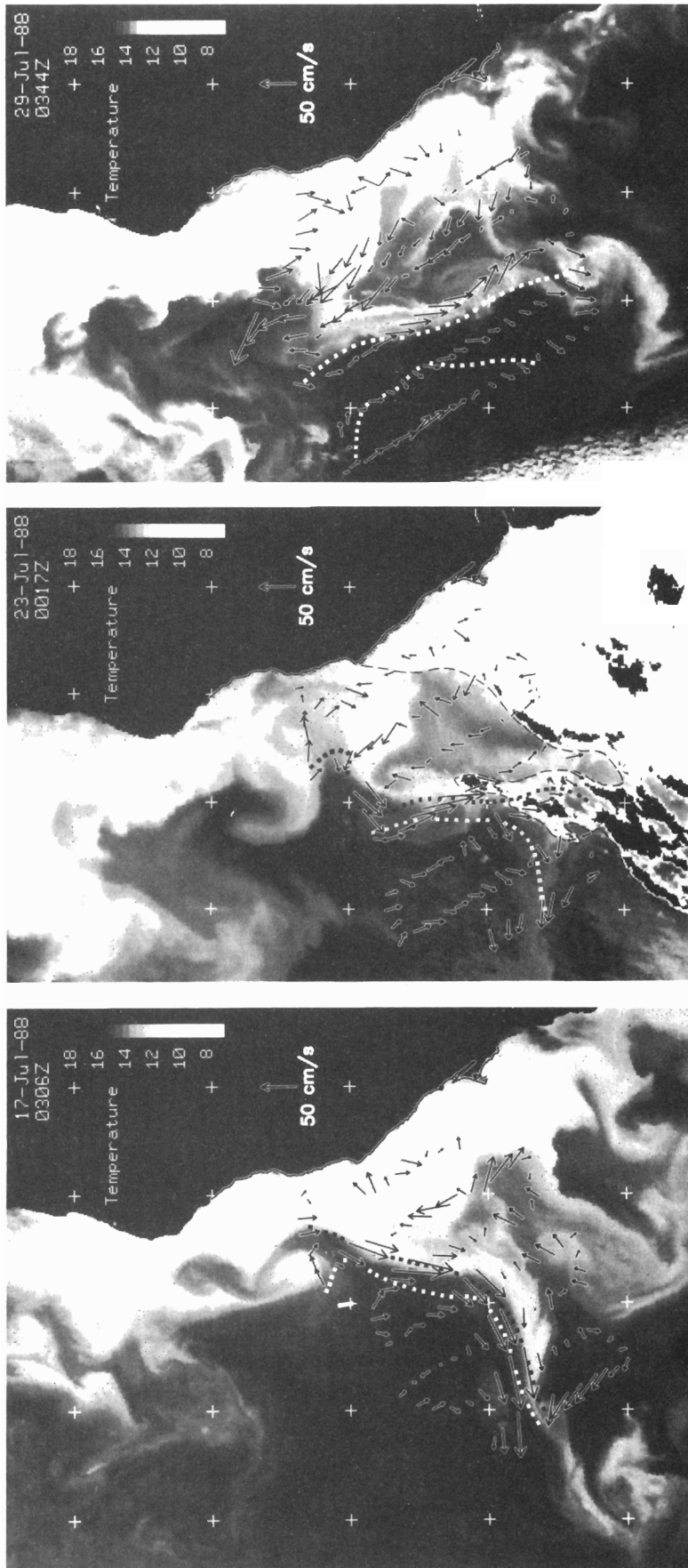
Fig. 3a

Fig. 3b

Fig. 3. Infrared (AVHRR) satellite images of sea surface temperature for the most cloud-free day near the midpoint of each complete survey. Superimposed on each image are the shipborne ADCP current vectors at 25 m, and the 8.6 and 9.4 m² s⁻² contours of geopotential anomaly at the sea surface relative to 500 dbar. (a) Images for June 27 and July 7, with current vectors measured during June 20–27 and July 6–12 respectively. (b) Images for July 17, July 23, and July 29, with current vectors measured during July 13–18, July 22–26, and July 29 to August 5, respectively. The southeastern portion of the July 23 image is obscured by a cloud bank whose edge extends southward from Point Arena.
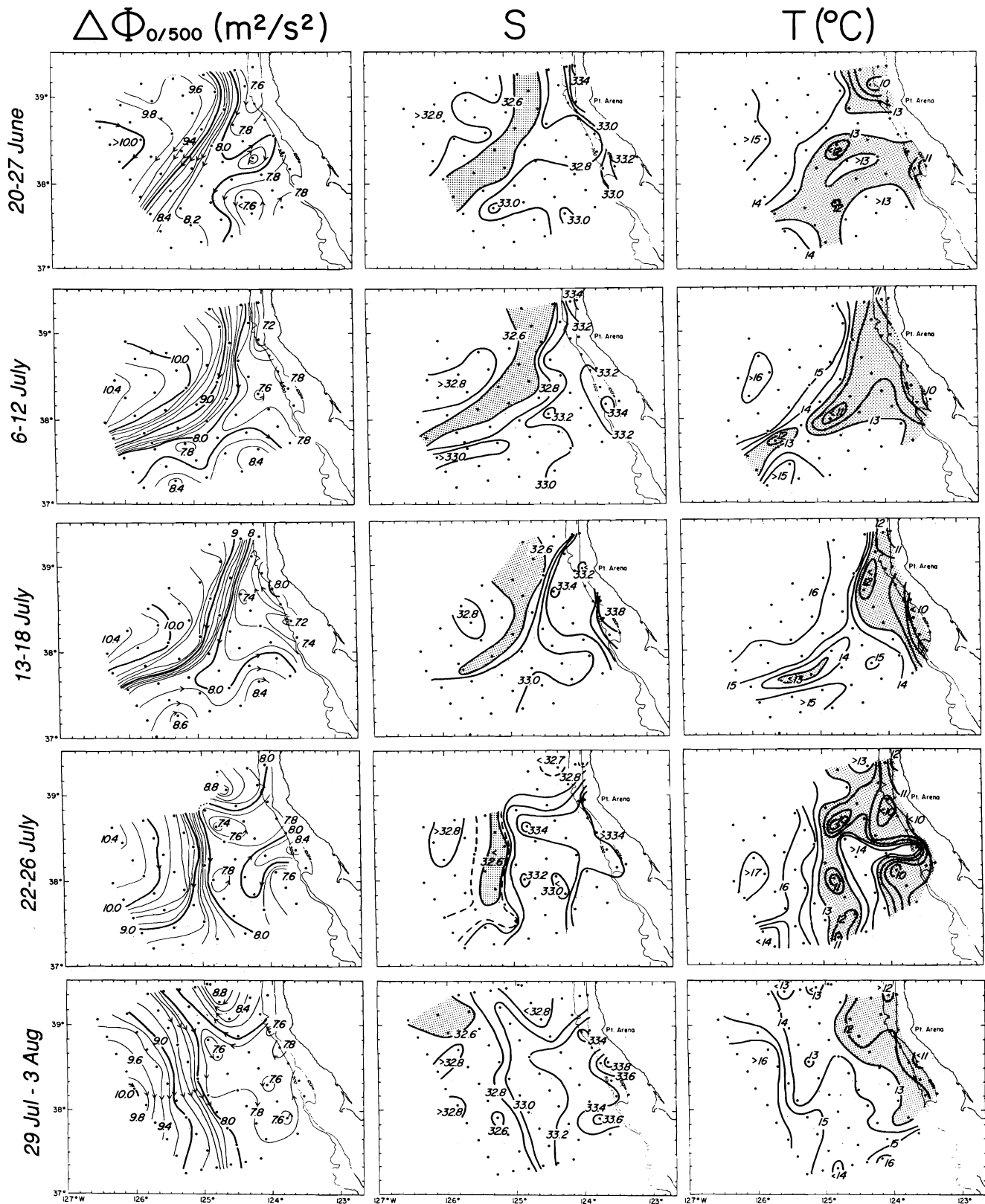
Fig. 4   Maps of the geopotential anomaly (relative to 500 dbar), salinity, and temperature of the sea surface for the five complete surveys made during June 20–27, July 6–12, July 13–18, July 21–27, and July 29 to August 3, 1988. Regions with surface salinity less than 32.6 psu or surface temperature less than 13°C are shaded. The 100- and 500-fm (180 and 900 m) isobaths are shown.
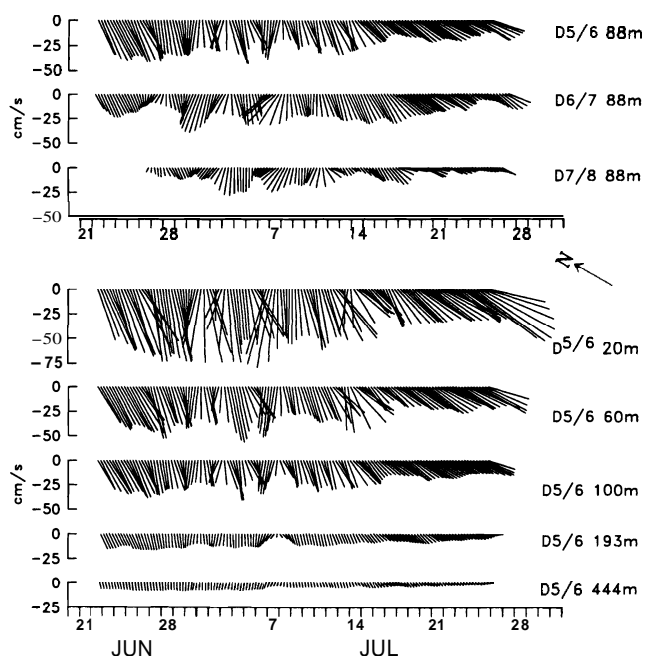
Fig. 5. (Top) Low-pass-filtered velocity vectors from 88 m below surface on moorings indicated in Figure 1. (Bottom) Low-pass-filtered velocity vectors from selected depths at mooring D5/6.

TABLE 2. Estimates of Volume Transport

	Alongshore Transport Through Line 5, Sv		Cross-Shore Transport Through Line F, Sv	
	Equatorward	Poleward	Offshore	Onshore
June 21–26	3.8	0.3	3.2	0.6
June 25 to July 2	3.7	...	3.9	0.7
July 6–12	3.9	0.6	4.2	0.5
July 13–17	4.0	1.0	3.7	0.6
July 22–26	3.6	...	2.5	0.2
July 29 to August 3	3.4	1.2	1.4	1.0

Estimates were obtained by integrating geostrophic velocity relative to 500 dbar through an offshore section (line 5, connecting F5, E5, D5, C5, B5 and A8), and through an alongshore section (line F). Only stations with CTD data to 500 m are included in the transport estimates. One sverdrup is equal to 10^6 m^3 s^{-1}.

Figure 4 shows the corresponding (hand-contoured) fields of the surface temperature T, salinity S, and geopotential anomaly (dynamic height) relative to 500 dbar ($\Delta\Phi_{0/500}$) as measured by the CTD over 5–7 days. The contours of geopotential anomaly would represent streamlines of geostrophic flow if the velocity at 500 dbar were everywhere zero. Selected contours of geopotential anomaly (the 8.6 and 9.4 m^2 s^{-2} contours) are included in Figure 3 to facilitate comparison with Figure 4.

The dominant feature of the surface velocity field throughout the survey sequence was a strong baroclinic jet, which was clearly observed in both the ADCP vectors (Figure 3) and the dynamic topography (Figure 4). The general position and orientation of the jet changed little during the first four surveys, i.e., between June 24 and July 15. During these surveys, the jet crossed the northern grid boundary near 39.2°N between 124° and 125°W and crossed the offshore boundary near 126°W between 38" and 39°N. Between the July 13–18 and the July 22–26 surveys a sharp meander apparently developed in the northeastern portion of the grid, but its structure was not adequately resolved by either survey. Time series of the velocity measurements at 90 m from the moorings along the D line (Figure 5) indicate that a change in the predominant direction of the current occurred between July 12 and 19. Near-daily D line sections (C. A. Paulson et al., manuscript in preparation, 1991) show that the jet orientation there changed from ENE-WSW to N-S between July 16 and 19. During the July 22–26 survey the jet was flowing nearly due south along 125°W between 38.7" and 37.8°N; farther south, the jet bifurcated, with part of the flow crossing the southern boundary at 37°N between 124" and 125°W and the remainder continuing offshore between 37° and 38°N as before. During the July 29 to August 3 survey, the jet was oriented primarily alongshore, with little net flow through the offshore boundary of the grid.

The strongest geostrophic velocities (>40 cm s^{-1} during all surveys) were generally observed somewhere between the 8.0 and the 9.6 m^2 s^{-2} contours of geopotential anomaly (Figure 4), but these contours were not always within the jet. For example, during the June 20-27 survey the 8.0 and 8.2 m^2 s^{-2} contours lay within the jet in the northeast portion of the grid but clearly inshore of the jet in the southern portion of the grid (Figure 4). Nevertheless, geopotential anomaly values between 8.6 and 9.4 m^2 s^{-2} occurred in or near the core of the jet throughout the survey sequence (Figure 3). The D5/6 mooring was between these contours during all but the last week of the deployment period; the median hourly speed at 20 m depth was 60 cm s^{-1}. The maximum current speeds measured by shipborne ADCP exceeded 100 cm s^{-1} during the July 13–18 survey and were weakest (63 cm s^{-1}) during the July 29 to August 3 survey (Figure 3). The cross-jet velocity profile was asymmetrical, with amplitude decreasing more slowly on the seaward flank than on the inshore flank; this was especially obvious during June 20-27 and July 6–12 (Figure 3). The jet was 30–50 km wide during the earlier surveys and perhaps 70 km wide during the last survey. Within some of the surveys (e.g., July 6–12 and July 22–26), the intensity and width of the jet varied downstream. Although the intensity, orientation, and width of the jet changed through the survey sequence, the equatorward baroclinic transport through the grid seemed to be remarkably constant at 3.5 to 4 Sv (Table 2). Transport estimates were also made by integrating the current measurements from the moorings, assuming that each mooring was representative of a 25-km portion of the jet cross section; during the period when the flow was nearly normal to the array, the transport through this 75-km-wide, 500-m-deep section was between 4 and 6 Sv with a mean for the period June 26 to July 13 of 4.8 ± 0.5 Sv.

On the offshore side of the jet (i.e., to the right facing downstream), the geopotential anomaly continued to increase to a maximum of >10.0 m^2 s^{-2} on the offshore boundary of our grid (Figure 4). If this maximum represented the core of an anticyclonic eddy, it would be a very large and persistent one (radius >150 km and time scale >6 weeks). It seems more likely that the gradient in geopotential anomaly continued offshore past the boundary of our survey grid: Wyrtki's [1974] map of the mean dynamic topography of the Pacific Ocean for May–June shows $\Delta\Phi_{0/500}$ increasing from
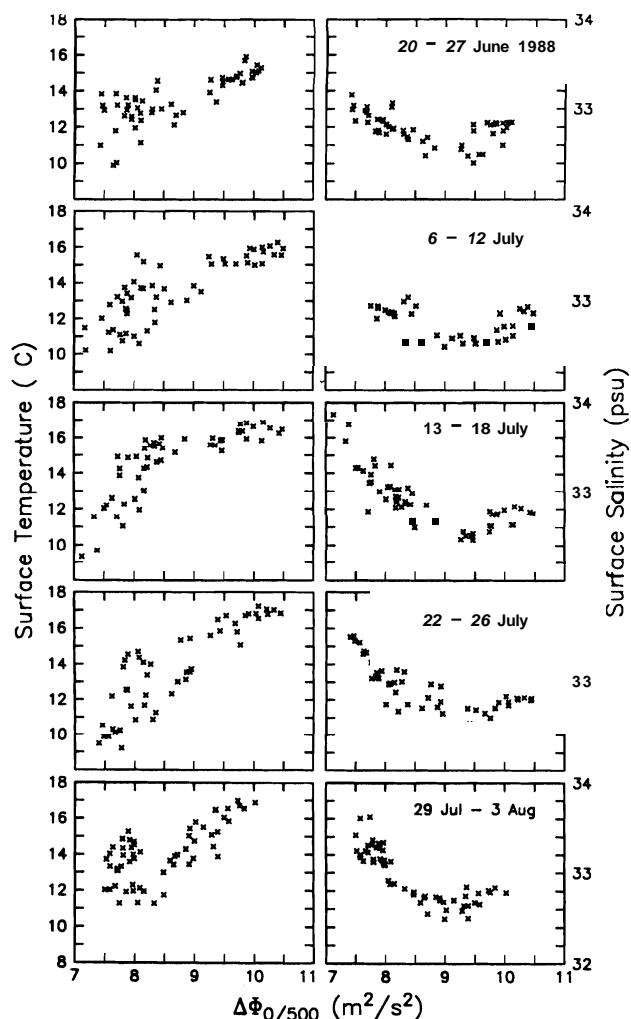
Fig. 6. Scatter plots of sea surface temperature and salinity versus the geopotential anomaly of the sea surface relative to 500 dbar, for each of the five complete surveys.

<8 m^2 s^{-2} along the northern California coast to about 12.5 m^2 s^{-2} near Hawaii.

Inshore of the jet, in the southeastern portion of the grid, eddies were more common. The maps of geopotential anomaly (Figure 4) suggest these eddies were small (radius <30 km) and ephemeral; it is difficult to identify the same eddy in two consecutive surveys. Confused ADCP vectors in the southeastern portion of the grid (Figure 3) indicate that our surveys did not generally resolve these eddies, either because of the sampling pattern or because of inherent noise.

The AVHRR images (Figure 3) show that the sea surface temperature distribution was extremely complex. Throughout the survey period, coldest waters ($<11°C$) occurred adjacent to the coast, and warmest waters ($>15°C$) occurred offshore, usually in the northwestern corner of the grid. In the transition region ($11°-14°C$), a tongue or filament of relatively cool water was associated with the core of the baroclinic jet. In general, the water at the core of the jet was not as cold as the coastal water, but small patches with temperatures of $<11°C$ observed during the 22–26 July survey (Figure 4) suggest localized mixing or upwelling along the jet. Some small-scale (<30 km) features in the AVHRR surface temperature fields (e.g., July 7) suggest the presence

of cyclonic and anticyclonic eddies on the flanks of the jet, but these were not resolved by our surveys. A larger anticyclonic eddy centered near 38.3°N, 124.0°W that was clearly resolved by ADCP and CTD measurements on June 22–23 is also visible (Figure 3a). In general, however, sea surface temperature reflects not only the mesoscale velocity field but also other superficial processes of short duration and small scales, such as internal waves, turbulence, and inhomogeneities in surface heating and mixing.

Scatter diagrams of surface temperature versus **geopotential** anomaly (Figure 6) show that minimum temperatures occurred in regions of low geopotential, inshore of the jet, while maximum surface temperatures occurred in regions of high geopotential, seaward of the jet. Similar scatter diagrams of chlorophyll and nutrients [Chavez et al., this issue, Figure **4**] suggest that the jet separated productive, recently upwelled, inshore waters from relatively barren waters offshore. Similar observations in June 1987 indicate that this flow regime extends at least 400 km along northern California, from **41.5°N** to 37.5°N [Hood et al., **1990**].

The maps of surface salinity (Figure 4) all indicate a tongue of low-salinity water tending equatorward on or near the axis of the jet and forming an absolute salinity minimum in the onshore-offshore direction. A very similar salinity minimum was observed in May 1987 [*Hayward* and *Mantyla*, 1990]. Strictly two-dimensional upwelling dynamics would result in a surface salinity field that decreases in the offshore direction, with the maximum salinity and temperature gradients coincident (or nearly so) along the upwelling front, but this was not observed. Scatter diagrams of salinity versus geopotential anomaly (Figure 6) show clearly that the gradients of temperature and salinity were not coincident and that the low-salinity tongue coincided with the region of geopotential gradient between the warm offshore waters and generally colder inshore waters. The simplest explanation is that the baroclinic jet advects fresher surface water southward from the north.

Subsurface Fields

The equatorward-tending jet dominated the baroclinic velocity field to depths of 200 m and more (Figure 7a). Throughout the survey sequence, the position and orientation of the jet did not change significantly with depth between the surface and 200 m (Figure 5, 7a); this similarity is reflected in the high pattern correlation coefficients for geopotential anomaly (Table 3). The vector maps (Figure 7b), the time series (Figure 5) and the regression coefficients of the geopotential anomaly fields (Table 3) all indicate that the intensity of the jet decreased by a factor of 5 or more. To depths of at least 100 m (Figure 7b), strongest measured currents occurred along the axis of the baroclinic jet. At 200 m the jet was still discernible, but currents of similar magnitude were also observed elsewhere. Velocity time series (Figure 5) from mooring **D5/6** near the axis of the jet show that the predominant direction of the current was unchanged between 20 m and 440 m, but current speeds at 440 m were reduced to less than 10% of their near-surface (20 m) value. This large reduction in speed indicates that 500 dbar is an appropriate choice of reference level for mapping geostrophic velocities.

Scatter diagrams (Figure 8) show that the relative minimum in surface salinity at the core of the jet did not usually
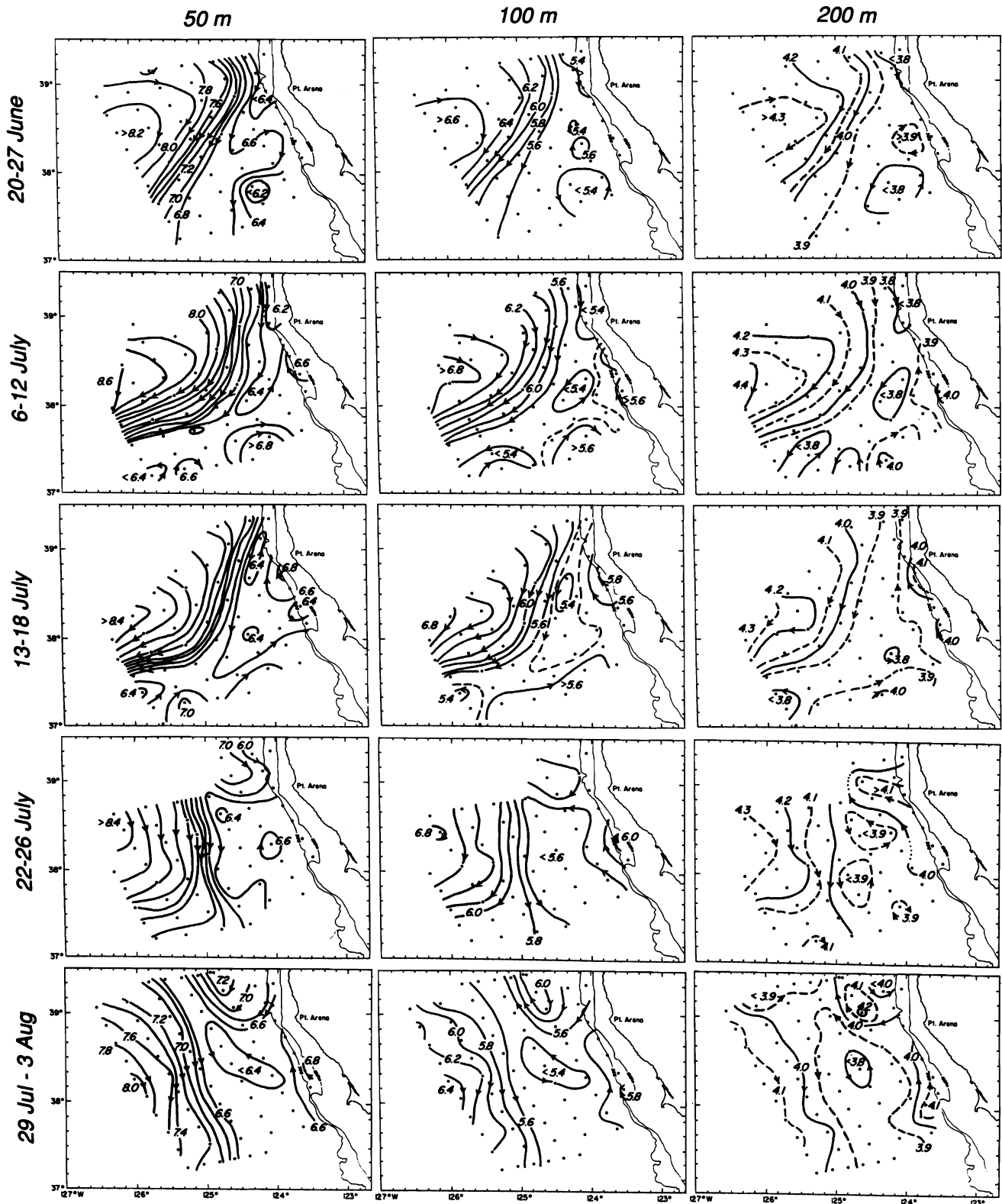
Fig. 7a. Maps of the geopotential anomaly (relative to 500 dbar) at 50, 100, and 200 dbar, for the five surveys during June 20–27, July 6–12, July 13–18, July 22–26 and July 29 to August 3, 1988. The 100- and 500-fm (180 and 900 m) isobaths are shown.

-extend to subsurface levels: at **50** m, salinities near the jet axis ($6.8 < \Delta\Phi_{0/500} < 7.8$ m^2 s^{-2}) were the same as those offshore, and at 100 m, salinity decreased monotonically across the jet. Similarly, the scatter diagrams for tempera-

ture (Figure 8) indicate that the complexity of the surface temperature field did not extend to subsurface levels: at both **50** and **100** m, temperature increased monotonically across the baroclinic jet.
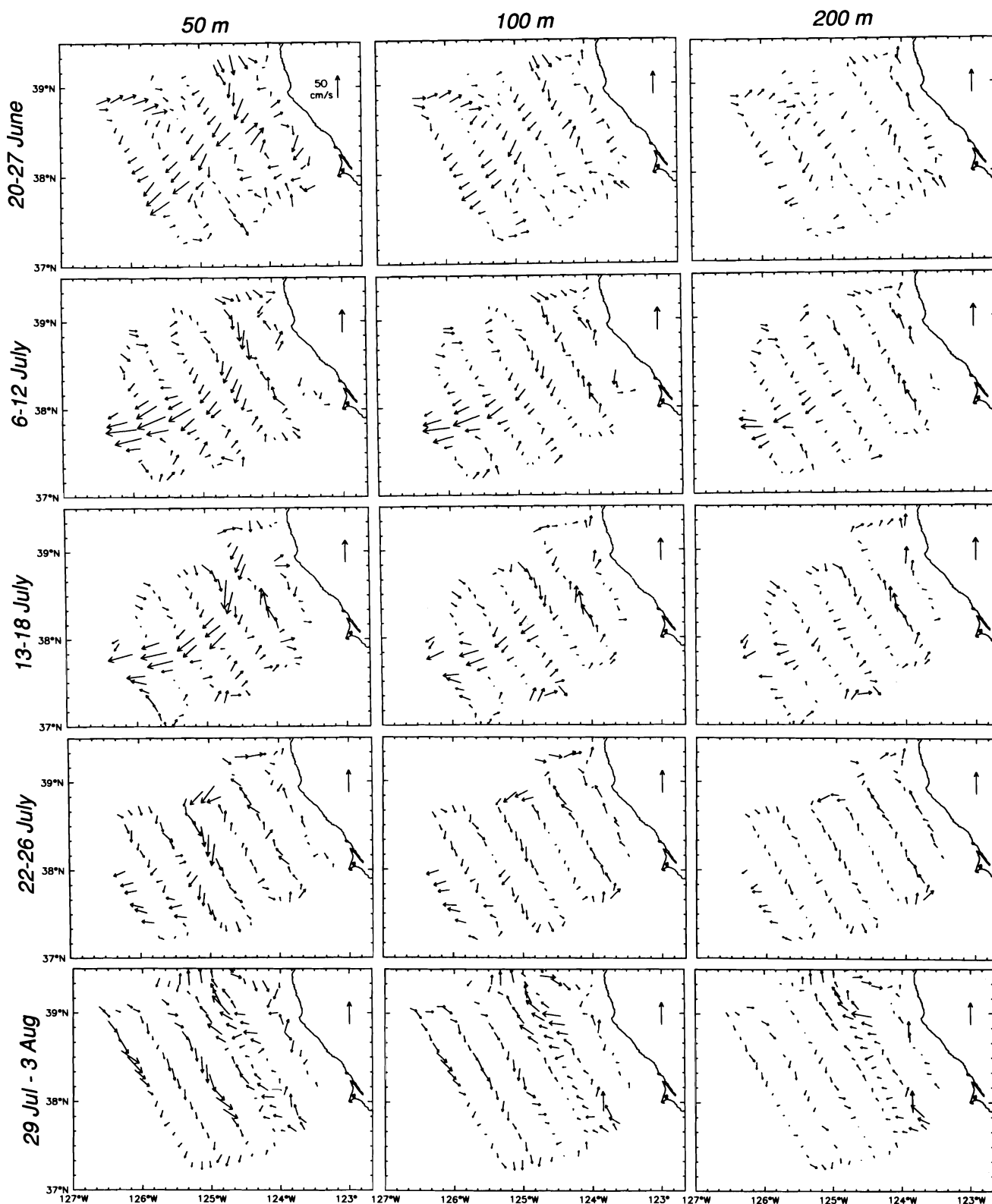
Fig. 7b. Maps of ADCP current vectors at 50, 100, and 200 dbar, during June 20–27, July 6–12, July 13–18, July 22–26, and July 29 to August 3, 1988.

The few eddies resolved by our surveys (e.g., at 38.4°N, 123.8°W, during June *20–27*) also seemed to decrease in intensity with increasing depth, with no significant change in position (Figures *7a* and *7b*). The position of maximum geopotential offshore of the jet was nearly independent of depth (Figure *7a*) and remained on the western boundary of the grid. Only a few of the small eddies inshore of the jet (Figures *3* and 4) were discernible at the 200 m level.

The one feature of the subsurface velocity fields (Figures *7a* and *7b*) not seen at the surface is the coherent **poleward**

TABLE 3. Linear Correlation and Regression Coefficients Between the Geopotential Anomaly at the Sea Surface and at Selected Depths, for the Five Complete Surveys

	June 20–27 (N = 55)	July 6–12 (N = 54)	July 13–18 (N = 52)	July 22–26 (N = 50)	July 29 to August 3 (N = 57)
	Correlation With $\Delta\Phi_{0/500}$				
$\Delta\Phi_{50/500}$	0.995	0.990	0.981	0.992	0.984
$\Delta\Phi_{100/500}$	0.987	0.973	0.947	0.968	0.928
$\Delta\Phi_{200/500}$	0.972	0.924	0.791	0.878	0.670
	Slope of Regression on $\Delta\Phi_{0/500}$				
$\Delta\Phi_{50/500}$	0.80	0.76	0.70	0.68	0.68
$\Delta\Phi_{100/500}$	0.55	0.50	0.43	0.42	0.38
$\Delta\Phi_{200/500}$	0.22	0.18	0.13	0.13	0.11

flow along the continental margin. The **poleward** flow was particularly obvious during the later surveys, when speeds up to 20 cm s^{-1} were measured at 200 m (Figure 76). Its structure was not resolved by our survey pattern, but previous onshore-offshore sections in this region show average **poleward** velocities of 10–15 cm s^{-1} along the bottom at depths of 150–200 m [*Kosro*, 1987; *Huyer and Kosro*, 1987]. This **poleward** flow presumably reflects the California Undercurrent, which has been observed at several latitudes between Baja California and British Columbia [*Huyer et al.*, 1989].

VERTICAL STRUCTURE

Onshore-offshore sections of the geostrophic velocity through the middle of our survey grid (Figure 9) show both the equatorward-tending surface current with its core lying 100–150 km offshore of the shelf break, and the **poleward** flow adjacent to the continental slope. In the onshore-offshore sections (Figure 9) the equatorward jet appears to be about 125 km wide, 2 or 3 times the width actually

observed in the surveys (Figures 3 and 4); this is largely due to the relatively coarse (40 km) onshore-offshore spacing between the alongshore sections of our survey grid, and also due to the oblique angle of intersection. The baroclinic volume transport (Table 2) of this equatorward flow was nearly constant (about 3.8 Sv) throughout the survey sequence, while the **poleward** transport increased from less than 0.5 Sv at the end of June to more than 1 Sv in early August; during the first month of the survey sequence, this equatorward transport also had an offshore component, with net offshore transport across the F line at the offshore boundary of the grid. An inshore equatorward surface current over the shelf break (Figure 9) was not adequately resolved by our surveys, but its presence was confirmed by current meters moored over the shelf by the Northern California Coastal Circulation Study (NCCCS) [*Magnell* et al., 1990]; it is also consistent with previous coastal surveys in this area [*Huyer and Kosro*, 1987]. The inshore currents over the shelf are highly variable [*Winant et al.*, 1987] and are not included in our transport estimates.
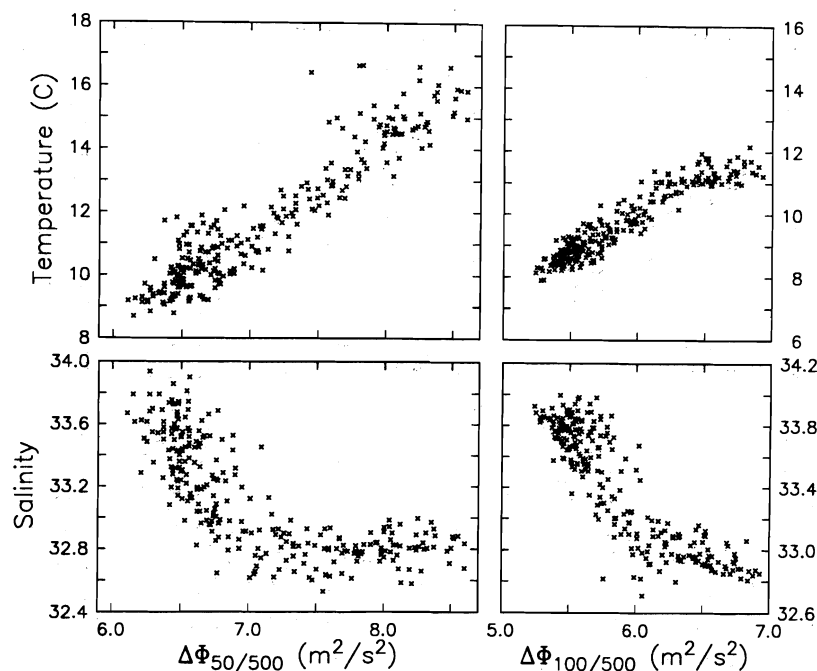

Fig. 8. Composite scatter plots of the temperature and salinity at (left) 50 and (right) 100 dbar versus the geopotential anomaly at the same depth (relative to 500 dbar).
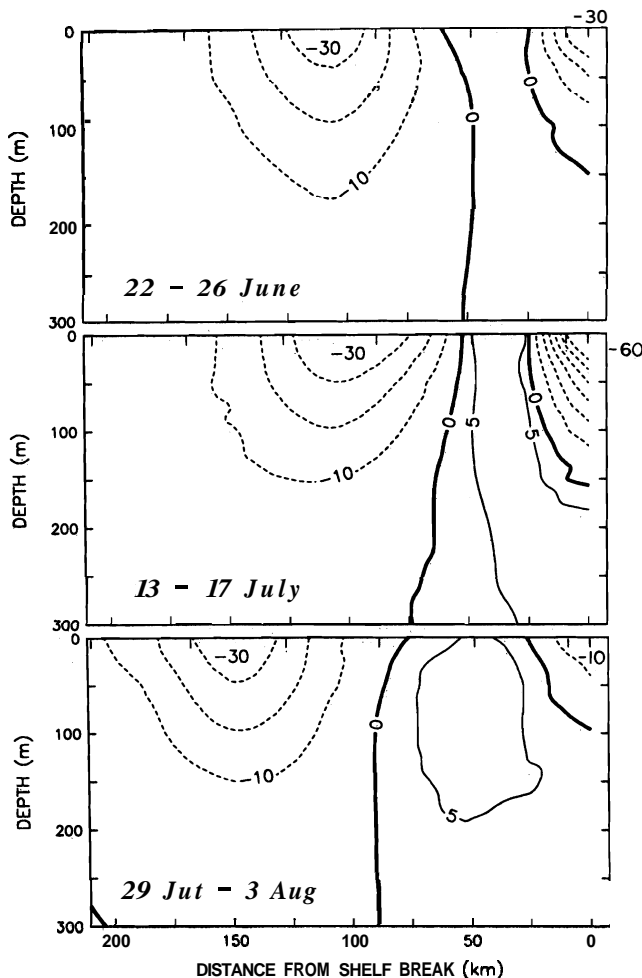
Fig. 9. Onshore-offshore sections of geostrophic velocity (relative to 500 dbar) along the line connecting F5 to B5, A8, and A9, at the beginning, middle, and end of the survey sequence.

A vertical cross section perpendicular to the equatorward jet (Figure 10) shows the characteristics of the jet clearly. Maximum measured (ADCP) current speeds at the core of the current are >70 cm s^{-1}, and the jet is about 50 km wide. Geostrophic velocity decreases with depth from more than 60 cm s^{-1} at the surface to less than 10 cm s^{-1} at 300 m. Also clearly visible are the coincidence of the jet axis with the $8.6-9.4$ m^2 s^{-2} band of $\Delta\Phi_{0/500}$, the near-surface temperature minimum centered just to the left of the jet axis, and the near-surface salinity maximum on the right flank of the jet (facing downstream). At subsurface levels (depths of >50 m), cross-jet gradients of temperature, salinity and density also generally decrease with depth, but they are still strong at 300 m; enhanced gradients are discernible even at 500, our maximum sampling depth. All of these characteristics are similar to those of seaward-tending jets observed in this region in July 1981 [Kosro and Huyer, 1986], July 1982 [Rienecker et al., 1985; Kosro and Huyer, 1986], and July 1986 [Rienecker and Mooers, 1989], as well as those of the meandering equatorward jet observed in May and June 1987 [Kosro et al., this issue; Ramp et al., this issue].

The distribution of geostrophic velocity (Figure 10) suggests that the jet is asymmetrical to a depth of at least 150 m. High-resolution cross-jet profiles of the near-surface current from the first survey (Figure 11) show cyclonic shears of

about $f/2$ (half the inertial frequency) and anticyclonic shears of about $f/10$; repeated sections along the D line show that the asymmetry was a persistent feature (Paulson et al., manuscript in preparation, 1991, Figure 3). A similar asymmetry was observed in July 1982 but not in July 1981 [Kosro and Huyer, 1986].

WATER MASSES OF THE TRANSITION ZONE

Temperature-Salinity Characteristics

The basic water mass structure in this region (Figure 12) is governed primarily by salinity and closely resembles Subarctic Water, whose characteristics have long been known [Tibby, 1941; *Tully* and Barber, 1960]. There is a definite halocline in which the density anomaly σ_θ increases from 25.2 to 26.5 kg m^{-3} and the salinity increases from about 33.0 to 33.8 psu. This halocline occurs at depths between 100 and 200 m offshore and often intersects the surface near the coast. Above the halocline (above $\sigma_\theta = 25.2$) is an upper layer whose salinity is nearly uniform with depth and whose temperature increases toward the sea surface from about 11°C at the top of the halocline; the salinity of this layer varies considerably from station to station. Below the bottom of the halocline (below $\sigma_\theta = 26.5$) lies a deep layer in which the salinity generally increases slowly with depth, although individual stations often exhibit small inversions in temperature or salinity, indicating patchiness and interleaving between water masses whose salinities differ by about 0.2 psu.

Lines of constant "spiciness" π, calculated from the algorithms provided by Flament [1986], are approximately parallel to the main trend of the mean T-S curve (Figure 12). ("Spiciness," a term coined by Munk [1981], is approximately orthogonal to the density anomaly σ_θ in the T-S plane; it is analogous to, but not identical with, the variable τ defined by Veronis [1972]). Low values of spiciness indicate a relatively high proportion of cool, fresh water; minimum values ($\pi = -0.2$) of the mean spiciness are observed near the top of the halocline (reflecting generally southward advection of near-surface low-salinity waters), and in the vicinity of the 26.8 isopcycnal (near the core of North Pacific Intermediate Water [Reid, 19651). The relatively high value of spiciness ($\pi > 0.0$) at the surface is due to regional heating: the long-term monthly mean heat flux is about 200 W m^{-2} downward through the sea surface at this time of year [Nelson and Husby, 1983]. Over the entire density range, mean values of spiciness are lower than those observed by Lynn and *Simpson* [1990] off southern California, in keeping with the climatological mean conditions which show cooler, fresher water to the north [Robinson, 1976].

Summary diagrams showing the T-S characteristics for all of the stations in each of the five complete grid surveys (Figure 13) show that the range of characteristics of the upper ocean waters ($\sigma_\theta < 26.5$) gradually increased with time between the first survey and the last. The general increase in the spiciness of the surface waters (Figure 13) is due to continued seasonal heating. At some stations this heating penetrated well into the halocline, though the minimum values of spiciness remain about the same throughout the halocline, indicating continued advection of relatively cool, fresh waters from the north. The deep water characacteristics ($\sigma_\theta > 26.5$) remained the same (Figure 13), and the average T-S curve for the survey region did not change appreciably during the sequence (Figure 14).
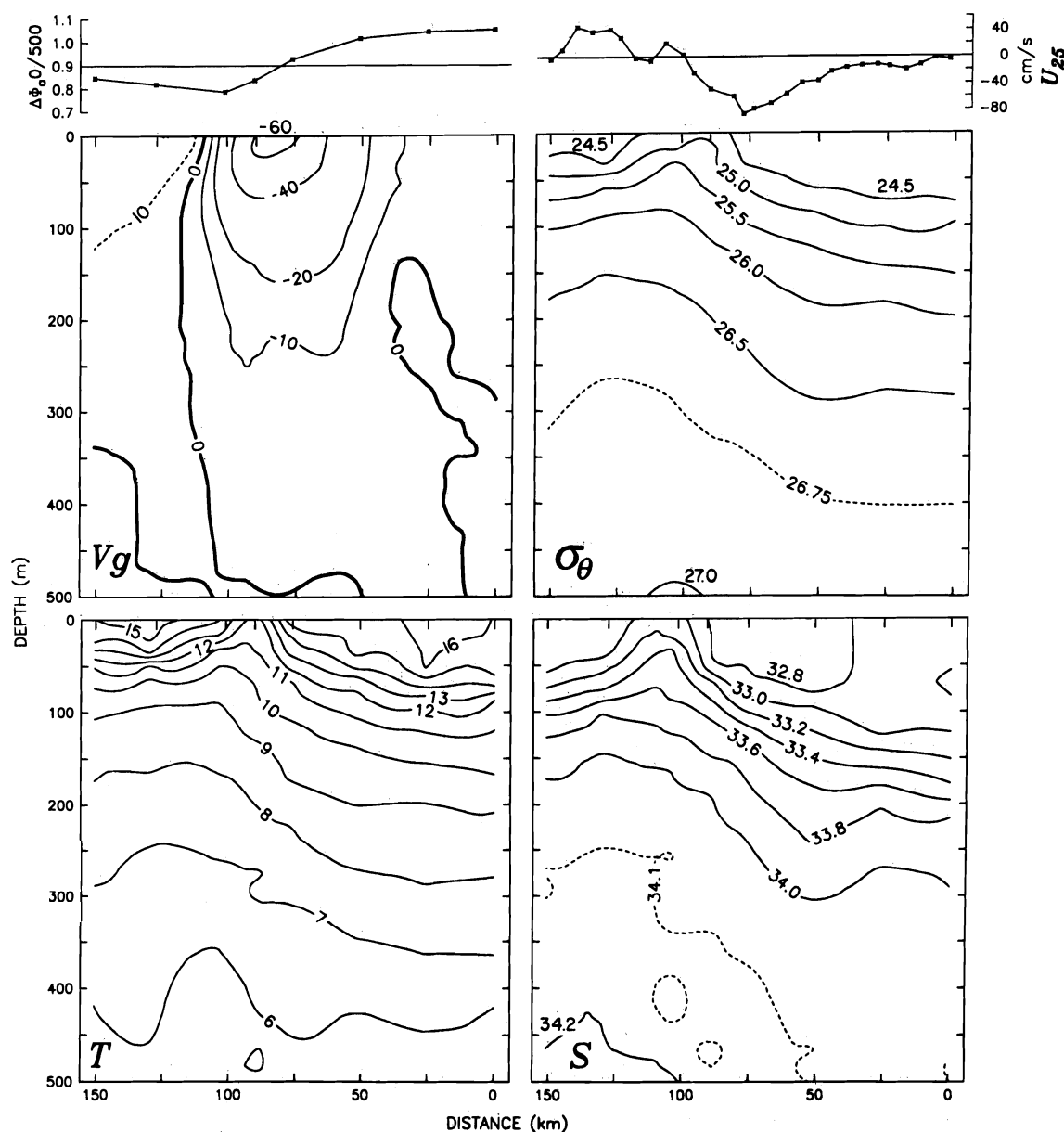
Fig. 10. The vertical cross-jet structure, facing downstream, of geostrophic velocity (negative downstream toward 240°T), temperature, salinity, and σ_θ along the F line on July 11–12, a time when the jet axis was approximately perpendicular to this section. Panels at the top show corresponding profiles of surface geopotential anomaly and the normal component of the directly measured (ADCP) current at 25 m averaged over 5 km. North is to the right.

The maps of surface temperature and salinity (Figure 4) for the five complete surveys suggested the possibility that the jetlike current flowing through the survey grid might be transporting a distinct water mass. To investigate this hypothesis, we divided the stations from each survey into three classes, defined by values of $\Delta\Phi_{0/500}$. To represent stations in the core of the jet, we chose a conservative $\Delta\Phi_{0/500}$ range of 8.6–9.4 $m^2 \, s^{-2}$; values as low as 8.0 $m^2 \, s^{-2}$ lie along the jet axis in some of the maps, but such values were also observed well away from the axis, possibly representing eddies or a portion of the onshore return flow. Similarly, we used stations with $\Delta\Phi_{0/500} < 7.8 \, m^2 \, s^{-2}$ to represent "inshore" waters and stations with $\Delta\Phi_{0/500} > 9.6 \, m^2 \, s^{-2}$ to represent "offshore" waters.

Averaged over all five complete surveys, the mean T-S curves for the inshore, offshore, and jet water masses are different, though by less than 1 standard deviation over most of their range (Figure 15). Within and above the halocline ($\sigma_\theta < 26.4$) the jet water mass is fresher (and cooler) than the offshore water, while both are significantly fresher than the inshore water mass (Figure 15). Averages calculated from individual surveys (Figure 16) yield similar results, with jet waters usually less spicy than both offshore and inshore waters (the jet and offshore waters were indistinguishable only during the July 22–26 survey). Since the surface temperature and salinity generally decrease with latitude in the California Current region [Huyer, 1983], these distinct jet characteristics reflect southward advection by a surface-trapped, equatorward jet. The characteristics of the jet waters are similar to those of the southward-flowing "northern waters" observed in this region in May 1987 [Paduan and Niiler, 1990]. An earlier study of the coastal upwelling
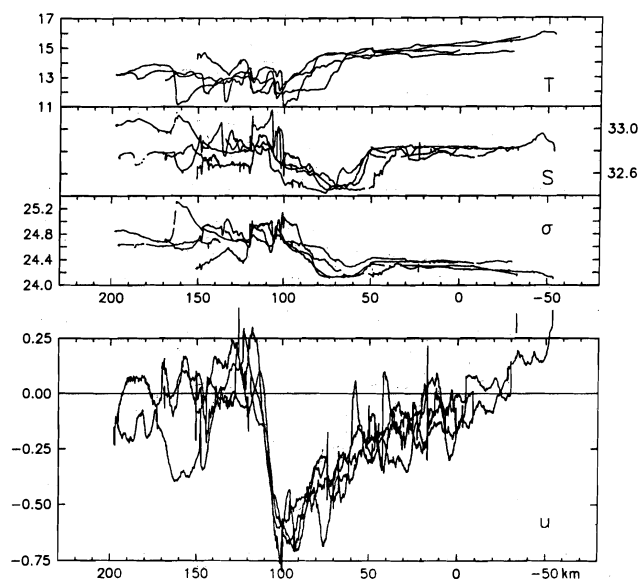
Fig. 11. (Top) Cross-jet profiles, facing downstream, of near-surface temperature, salinity, and σ_θ (all at 4 m), and (bottom) normal component (toward 060°T) of directly measured (ADCP) velocity at 21 m (negative velocity downstream toward 240°), along the C, D, E, and F lines, during the June 20–27 survey. Each profile shows values at 5-min intervals along the ship's track; the velocity data have been filtered by averaging over 30 min. Profiles have been shifted left or right so that the maximum horizontal velocity gradients coincide on the horizontal axis. North is to the right.

(Figure 18) are equivalent to maps of temperature or salinity; Table 4 provides the values corresponding to each spiciness contour for the three isopycnals. The geostrophic flow along each isopycnal surface (Figure 19) is proportional and normal to the gradient of the "acceleration potential" as formulated by Reid [1965].

The $\sigma_\theta = 25.8$ surface is the shallowest isopycnal that does not intersect the sea surface seaward of the continental shelf; it is tilted steeply up toward the coast, with the strongest slopes on or near the axis of the jet in each survey (compare Figures 17 and 19). Minimum values of spiciness generally coincide with the axis of the equatorward current, but the correspondence is not perfect. During the first survey, the low-spiciness tongue lay just inshore of the axis of the current; perhaps the current axis was propagating rapidly offshore at this time. Through most of the survey sequence, the shape and position of the low-spiciness tongue were consistent with the changing position of the equatorward jet (compare Figures 18 and 19). The persistence of this low-spiciness tongue is remarkable: along-jet velocities of >20 cm s^{-1} at this depth (Figure 19) imply equatorward displacements of >150 km between consective surveys and >500 km between the first and last surveys; in spite of these large displacements, the minimum values of spiciness vary only slightly from survey to survey. In one sense, the property distribution in the jet is approximately two dimensional: cross-jet gradients of spiciness (−0.2120 km) are much greater than along-jet gradients (≈0.2/500 km). Note, however, that the jet axis waters are not perfectly homogeneous:

region off central Oregon (45°N) had indicated southward advection of Subarctic Water through the coastal jet along the upwelling front over the shelf [Huyer and Smith, 1974]; the regime here seems to be similar.

Below the halocline ($\sigma_\theta > 26.5$), the mean jet and offshore T-S curves are indistinguishable, but the inshore water is relatively warm and saline (Figure 15). Averages from individual surveys show that the inshore waters were spicier than the offshore and jet waters throughout the survey sequence (Figure 16). The high spiciness of the inshore waters reflects poleward advection along the continental margin through the California Undercurrent.

Isopycnal Analysis

Although the average T-S curves of the inshore, jet, and offshore waters (Figures 15 and 16) are distinct over a large portion of the overall density range, their standard deviations indicate significant overlap. To determine whether the transition between water masses was abrupt or gradual, and whether the variation within each water mass was smooth or patchy, we examined the spatial distribution of water mass characateristics on isopycnal surfaces. In this region of the ocean, isopycnal surface lie within a few meters of the "neutral surfaces" along which fluid particles can move and mix without having to supply gravitational potential energy [*McDougall*, 1987]. We chose three surfaces to represent waters of the upper halocline ($\sigma_\theta = 25.8$ kg m^{-3}), the lower halocline ($\sigma_\theta = 26.2$), and the Intermediate Water below the halocline (a, = 26.8). The upper surfaces are separated vertically by about 50 m, and the lower surfaces are separated by about 200 m (Figure 17). The maps of spiciness
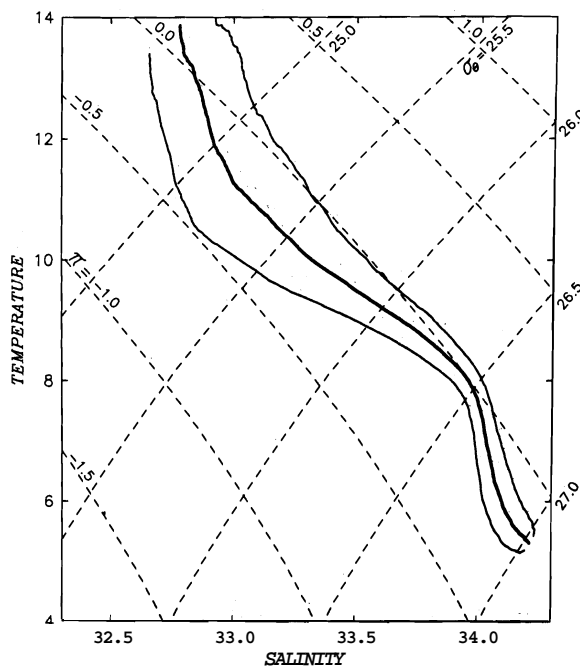

Fig. 12. The overall average T-S curve of the 283 stations along the A-F lines during the five complete surveys, calculated as a function of density (σ_θ interval of 0.01 kg m^{-3}), and the curves showing the average plus and minus 1 standard deviation. Curves are shown only for the density range covered by at least 10 stations. Dashed curves sloping up toward the right are lines of constant density anomaly (σ_θ), and dashed curves sloping down to the right are lines of constant spiciness (π).
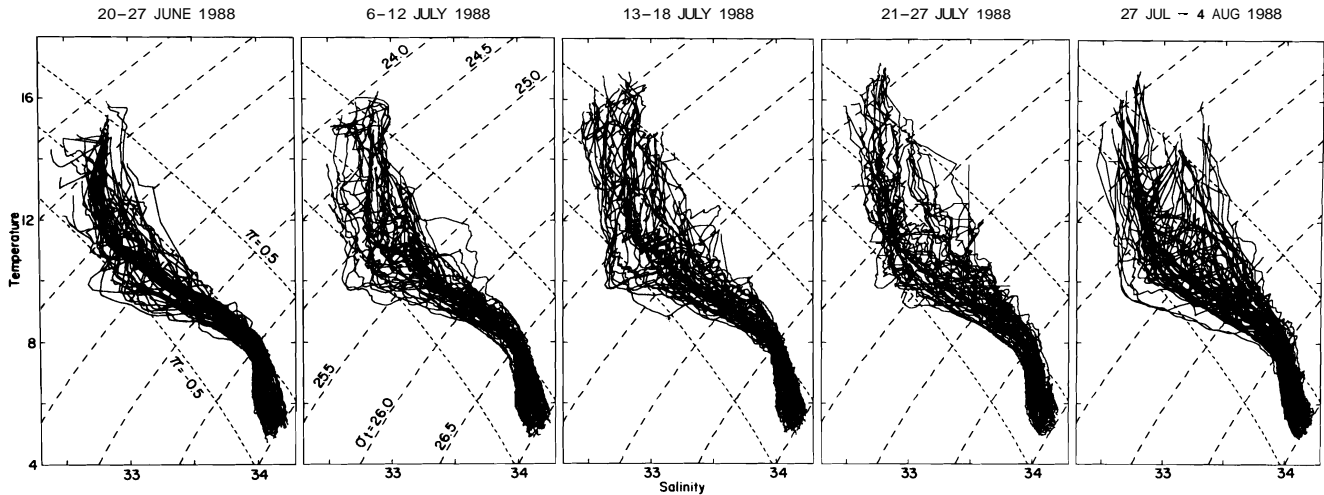
Fig. 13. *T-S* curves for all stations during each complete survey. Dashed curves sloping up toward the right are lines of constant density anomaly (σ_θ), and dashed curves sloping down to the right are lines of constant spiciness (π).

there is some patchiness with along-jet scales between 10 and 50 km, and as much variation within each survey as between surveys.

Both inshore and offshore of the jet, waters on the 25.8 isopycnal were moving sluggishly, with geostrophic velocities generally less than 10 cm s^{-1} (Figure 19). Offshore of the jet, this isopycnal lies at depths of >140 m, well below the influence of surface heating and wind mixing, and spiciness values there (-0.1 to -0.2) did not change appreciably during the sequence. However, inshore of the jet, this isopycnal lay near the sea surface (depths of <80 m), and the spiciness increased appreciably, consistent with the long-term mean monthly heat flux which is downward through the

sea surface at this time of year *[Nelson* and *Husby,* 1983]. The extreme patchiness of spiciness in this inshore region indicates that the downward penetration of surface heating occurs through processes with small horizontal scales (<10 km), such as breaking internal waves; this is consistent with turbulence measurements farther north near Cape Blanco *[Mourn et* al., 1988].

The $\sigma_\theta = 26.2$ isopycnal near the bottom of the halocline also rises steeply upward toward the coast (Figure 17). Previous studies in this region [e.g., *Huyer,* 1984] show that this isopycnal frequently intersects the sea surface over the
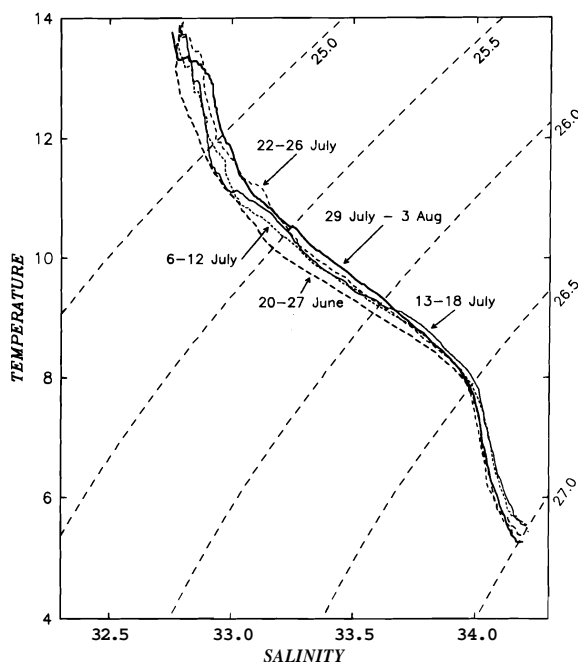

Fig. 14. Average *T-S* curves for each of the five complete surveys. Curves are shown only for the density range covered by at least 10 stations.
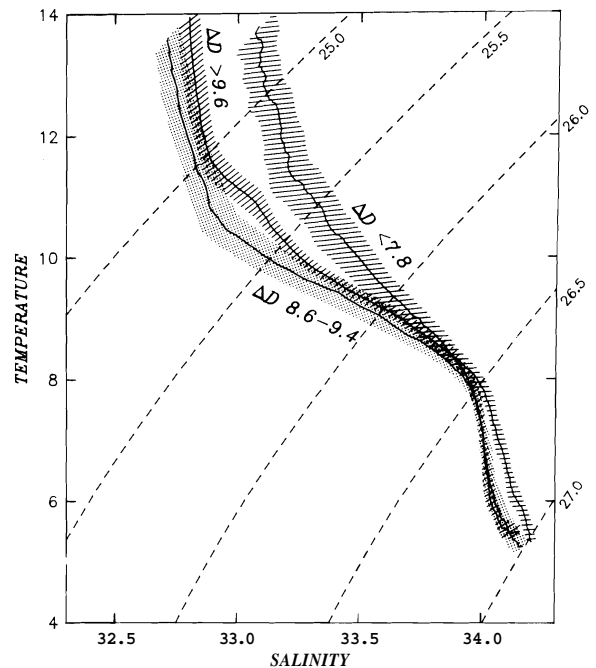

Fig. 15. Average *T-S* curves for three groups of stations from the five complete surveys: "inshore," "offshore," and "jet core," defined by three ranges of dynamic height ($\Delta\Phi_{0/500} < 7.8$, $\Delta\Phi_{0/500} > 9.6$, and $9.4 > \Delta\Phi_{0/500} > 8.6$, respectively). Hatched or shaded areas show the region within one-half standard deviation of the means.
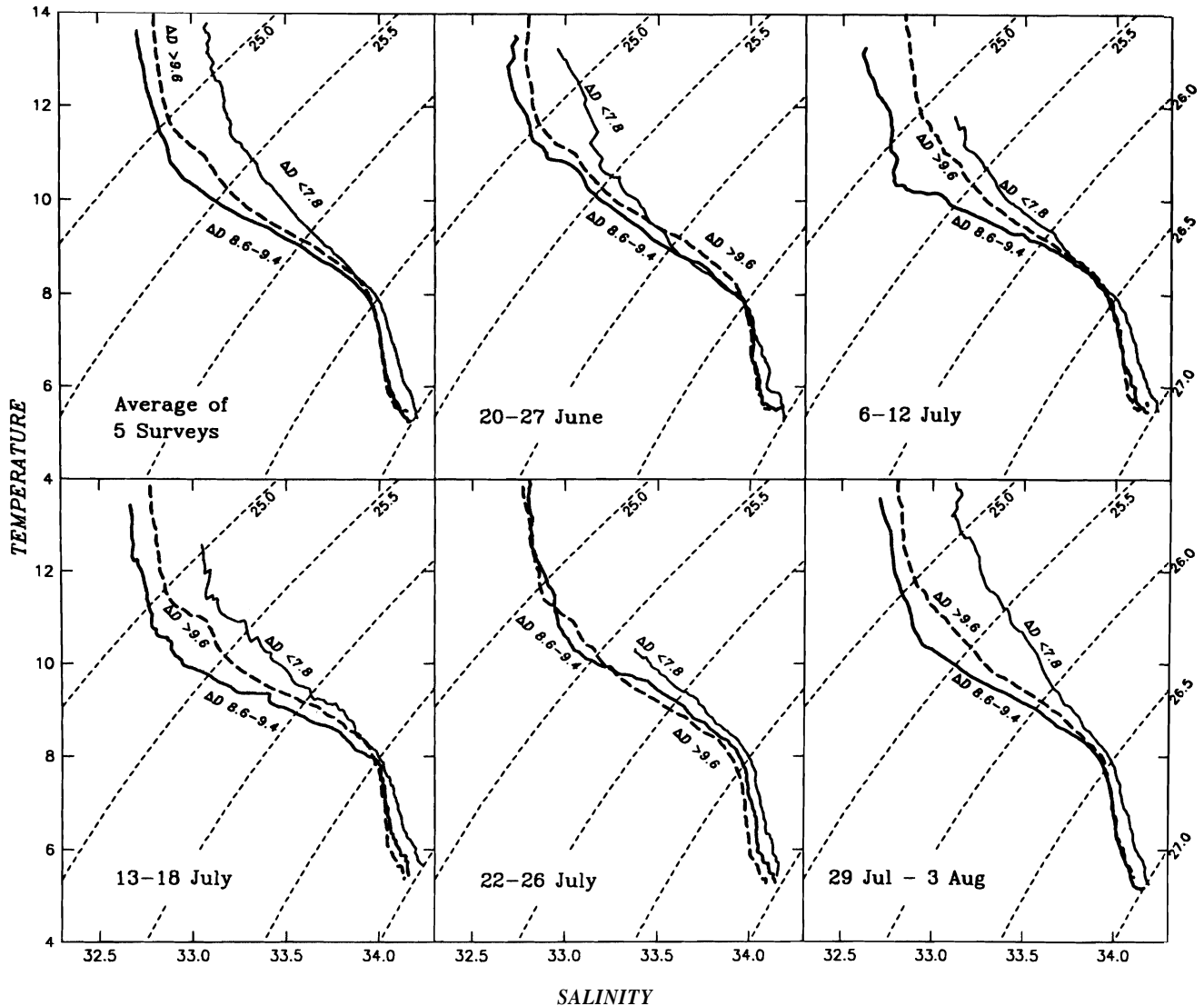
Fig. 16. Average T-S curves for the inshore, offshore, and jet core stations for each of the five surveys. Curves are shown only for the density range covered by at least four stations. (The top left panel repeats the average curves of Figure 15 for comparison).

inner shelf. The equatorward flow on this surface (Figure 19) is reduced to about 60% of the flow at $\sigma_\theta = 25.8$; the weaker flow may contribute to the small range (and higher values) of the spiciness on this surface (Figure 18). Nevertheless, minimum values of spiciness still occur on or near the axis of the current and remain about the same throughout the sequence. The highest values of spiciness inshore of the equatorward current seem to be associated with northward flow along the continental margin (compare Figures 18 and 19). There is little indication of local heating on this isopycnal, and the spiciness distribution is much less patchy than in the upper halocline (at $\sigma_\theta = 25.8$).

The $\sigma_\theta = 26.8$ isopycnal lies at the core of North Pacific Intermediate Water, which has its origins in the northwestern Subarctic Pacific [Reid, 1965]. Even within our survey region, the $\sigma_\theta = 26.8$ isopycnal shows a general gradation in spiciness, with offshore values lower than those near the margin, consistent with equatorward flow in the offshore portion of the grid and poleward flow along the continental

margin. The depth range of this isopycnal during our surveys (300 to 450 m) is similar to that expected from Reid's ocean-scale map (his Figure 17), which shows depths of about 300-400 m along the coast from Vancouver Island to Baja California. Our first survey shows the isopycnal rising nearly monotonically toward shore, but later surveys show a definite ridge about 100 km from shore (Figure 17); this ridge can also be seen in Reid's large-scale map. The deepening of the isopycnal toward the coast is consistent with poleward flow along the continental margin (Figure 19) and indicates that the core of the undercurrent lies above this surface, that is, shallower than 400 m. The maps of acceleration potential (Figure 19) suggest that this poleward undercurrent strengthened during the survey sequence. Both the core depth and the flow intensification are consistent with direct current measurements at the NCCCS mooring over the upper slope [Magnell et al., 1990] and also with 1981 and 1982 data from the C5 mooring over the upper slope at 38.7°N [Huyer et al., 1989; Lentz and Chapman, 1989].
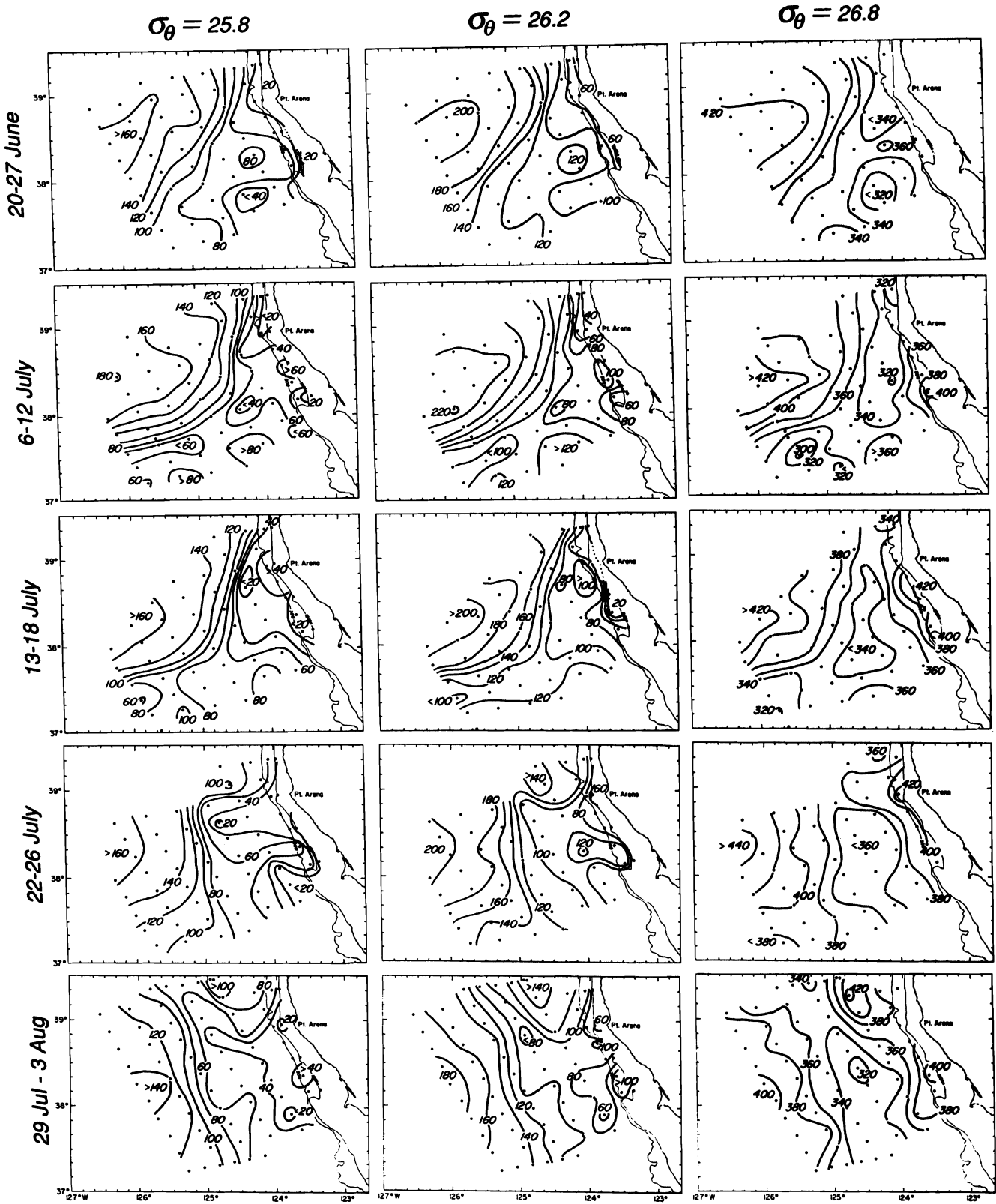
Fig. 17.   Depth (meters) of the isopycnal surfaces on which σ_θ is **25.8, 26.2,** and **26.8,** for the **five** complete surveys.

DISCUSSION

Change in Jet Axis Position

During the first half of the survey sequence, the position and orientation of the jet axis (as marked by the **9.0** m^2 s^{-2}

contour of $\Delta\Phi_{0/500}$) remained essentially the same, but between the July 13–18 and July **22–26** surveys, the jet changed orientation, moving offshore in the northern portion of the grid, and onshore in the southern portion (Figure **20**). This trend of the jet axis migrating to a more-alongshore
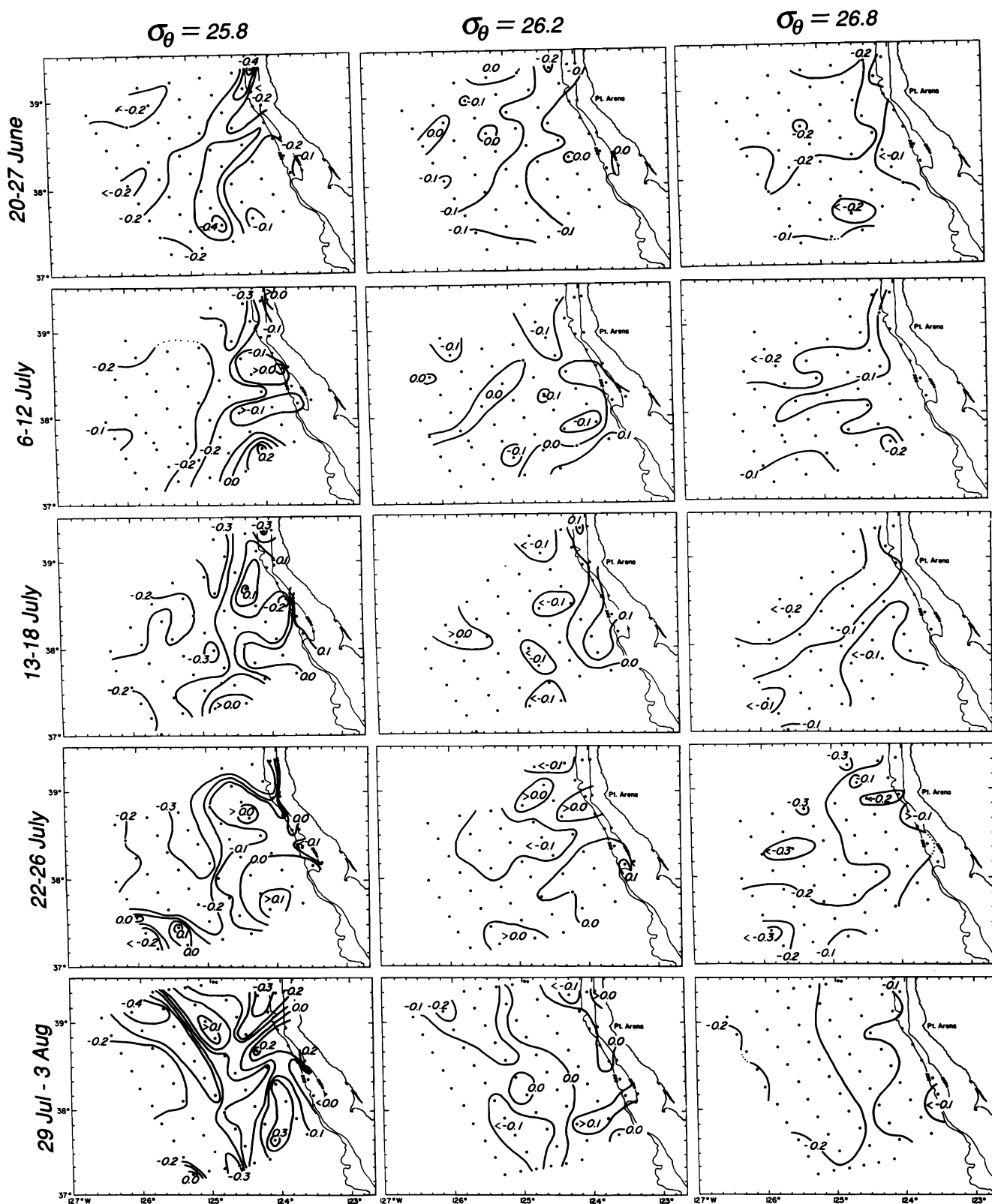
Fig. 18. Spiciness on the isopycnal surfaces on which σ_θ is 25.8, 26.2, and 26.8, for the five complete surveys.

orientation continued between the July 22–26 and the July 29 to August 3 surveys. At about the same time, i.e., in mid-July, the intensity of the jet decreased, and its width increased, although the total transport relative to 500 dbar remained about the same (Table 2). There is a suggestion in

Figures 4 and 7a that the change occurred earlier on the inshore flank of the jet: at both surface and subsurface levels, the values of geopotential anomaly in the northwest remain about the same between the July 13–18 and July 22–26 surveys, while those in the southwest increase signif-

TABLE 4. Values of Temperature and Salinity at Selected
Values of Spiciness π, on the Isopycnal Surfaces With σ_θ
Values of 25.8, 26.2, and 26.8 kg m^{-3}

π	$\sigma_\theta = 25.8$		$\sigma_\theta = 26.2$		$\sigma_\theta = 26.8$	
	T	S	T	S	T	S
−0.4	8.9	33.28	7.5	33.53	5.3	33.91
−0.3	9.2	33.33	7.9	33.59	5.7	33.97
−0.2	9.5	33.40	8.2	33.66	6.1	34.04
−0.1	9.8	33.47	8.6	33.73	6.5	34.10
0.0	10.1	33.53	8.9	33.79	6.8	34.16
0.1	10.4	33.59	9.2	33.85	7.2	34.23
0.2	10.7	33.66	9.5	33.92	7.6	34.29
0.3	11.0	33.71	9.8	33.97	7.9	34.35
0.4	11.2	33.79	10.1	34.04	8.2	34.42

icantly. Thus the bifurcation of the jet seen in the July 22–26 survey (Figure 4) may be a transient feature associated with the reorientation.

Why did this change in orientation and position occur? Since it occurred only once during the survey sequence, we cannot provide a definite answer. However, a very similar change was observed in July 1986 [*Rienecker and Mooers,* 1989; *Mooers,* 1989], and some possible explanations are worth discussing. The velocity records from the moorings provide more precise timing of the change in the jet's direction. The directions of the velocity vectors from several depths on the D line moorings (Figure 21) show that the change in the jet's direction near the center of the grid occurred during July 11–18, prior to the reversal of the coastal winds on July 18. Coastal sea level and the currents at midshelf (measured by the NCCCS program [*Magnell et al.,* 1990]) did respond to the change in coastal winds but the jet, well seaward of the shelf, was unaffected. The change in the direction of the jet did coincide with a distinct change in the currents over the inner slope (the 400-m NCCCS mooring at 38.5°N [*Magnell et al.,* 1990]). The currents at 10, 75, and 150 m showed strong poleward acceleration between July 11 and 14; the 75- and 150-m currents became poleward on July 12 and remained steadily poleward for the next month. As the poleward flow passes Point Arena, where the isobaths turn abruptly, it may cross isobaths, gain relative vorticity, and turn offshore, with the result that the upwelling front would be displaced offshore in the northern part of the grid. If this strengthening of the undercurrent is an annual occurrence (as is suggested by the seasonal variation of a year-long record of currents at this location [*Huyer et al.,* 1989]), it could also explain why a similar change in jet position and orientation occurred in July 1986.

Another possibility is forcing by the wind stress curl. Positive curl would result in increased upwelling and, presumably, offshore migration of the upwelling front. Wind data from *Wecoma* indicate that the curl was near zero during the first survey [*Fleischbein et al.,* 1988] and generally positive during the last survey [*Kosro et al.,* 1988]. We do not know the curl field in sufficient detail to determine whether it is consistent with the rotation of the jet in mid-July 1988.

Finally, inspection of all available satellite infrared images suggests that eddy-jet interaction may be important. The imagery suggests that the inflow across 39.3°N was seriously disrupted sometime between July 17 and 28. The images for

June 27 and July 7 show a strong continuous cold front extending from well north of Cape Mendocino (at 40.3°N) southward into the offshore jet. On July 14, two cold eddies appear as "dog ears" protruding from the cold front near Cape Mendocino. By July 15 the more southern cyclonic eddy had strengthened considerably and moved southward to about 39.5°N, 124.7°W, and a small perturbation had appeared on the cold front due east of the eddy. By July 16 this perturbation had grown and a strong eddy-jet interaction was evident, in which the eddy was entraining cold water from the coastal region. This process continued on July 18, when the front was displaced well offshore by the cyclonic eddy. This apparent eddy-jet interaction process might explain the continued offshore displacement of the jet.

California Current or Coastal Jet?

The California Current is traditionally described, on the basis of historical hydrographic data, as a broad and weak surface current that carries low-salinity water southward from the subarctic Pacific [e.g., *Reid et al.,* 1958; *Wooster and Reid,* 1963; *Hickey,* 1979]. For the region south of San Francisco, *Chelton* [1984] and *Lynn and Simpson* [1987] have calculated seasonal variations in the structure of the California Current from repeated surveys of the large-scale California Cooperative Oceanic Fisheries Investigations (CalCOFI) grid. Off San Francisco the core of the long-term average California Current in July lies 350 km offshore, at about 36.5°N, 126°W (between CalCOFI stations 60.90 and 60.100); at this location there is a local minimum (about 32.95 psu) in the mean July profile of surface salinity and a local maximum (8–10 cm s^{-1}) in the seasonal equatorward current [*Lynn and Simpson,* 1987]. The position of this large-scale salinity minimum and velocity maximum is only about 100 km southwest of the CTZ survey grid, and drifters deployed inside our baroclinic jet [*Brink et al.,* this issue] passed on either side of it. The station spacing of the CalCOFI grid (74 km) is almost twice the spacing between the alongshore sections of the CTZ grid (Figure 9); thus even individual CalCOFI surveys would seriously underestimate the speed of a narrow current. It is plausible, then, that the equatorward baroclinic jet observed in the CTZ surveys is identical with the core of the California Current.

At the northern boundary of the 1988 CTZ survey grid, the structure and intensity of the baroclinic jet resembles the coastal jet observed in the upwelling region off central Oregon [*Mooers et al.,* 1976; *Huyer et al.,* 1979], except that the latter lies over the middle and outer shelf. As noted above, both the coastal jet off Oregon and the baroclinic jet in the CTZ region seem to advect water with characteristics of a more northerly origin equatorward. Continuity between jets at locations so far apart will be difficult to establish with the data now available. Further questions regarding the origin and the nature of the equatorward jet are discussed by *Kosro et al.* [this issue] and *Strub et al.* [this issue].

CONCLUSIONS

Repeated mesoscale surveys of the coastal transition zone off northern California during summer 1988 all showed the presence of a strong, surface-intensified equatorward jet. Strongest velocities (>50 cm s^{-1}) occurred between geopotential anomaly contours of 8.6 and 9.4 m^2 s^{-2}. In late June
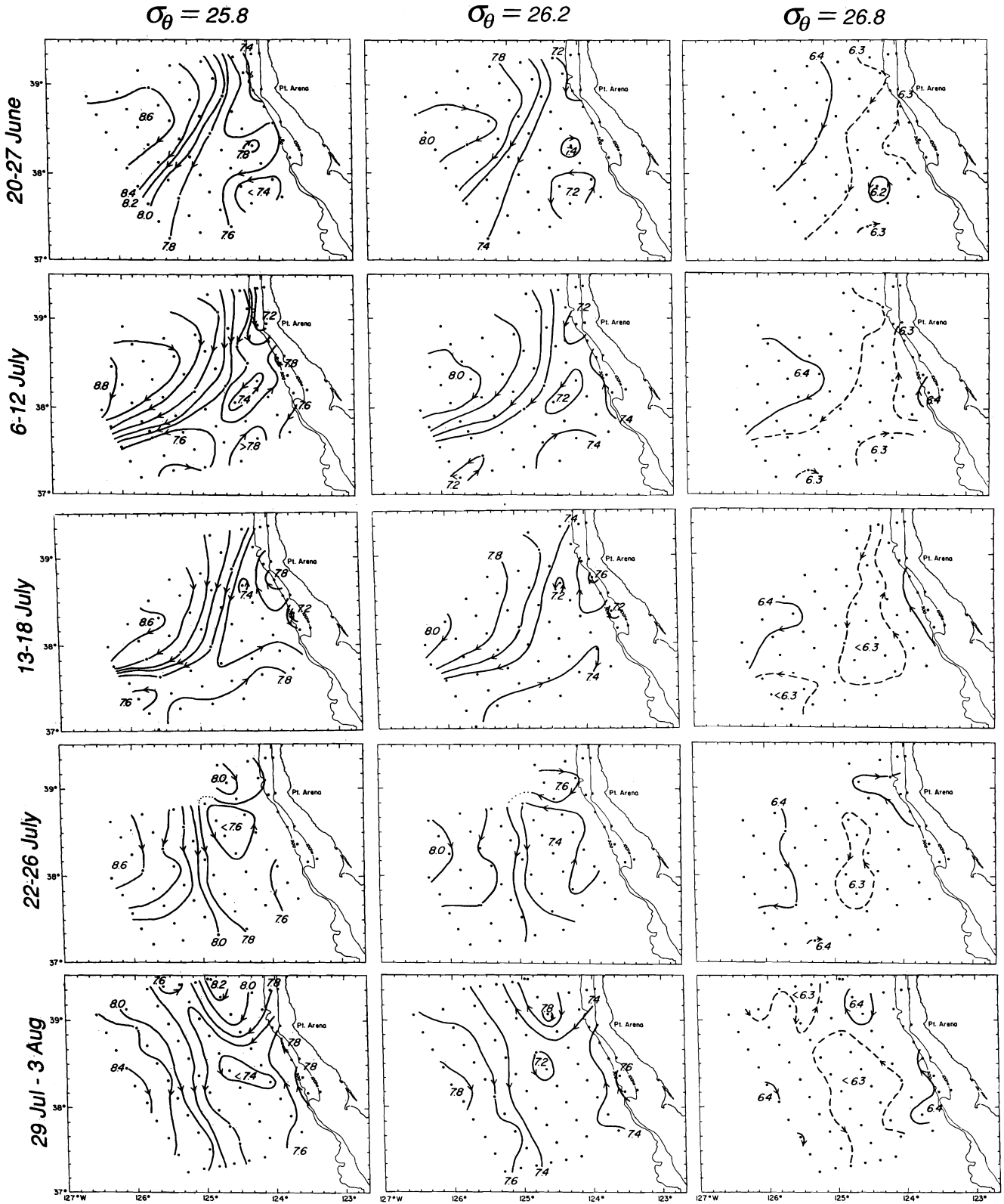
Fig. 19.   Acceleration potential (m² s⁻²) on the isopycnal surfaces on which σ_θ is *25.8, 26.2,* and *26.8,* for the five complete surveys.

the core of this current lay about 70 km offshore from Point Arena and more than 200 km offshore from Point Reyes. The jet remained in about the same position from late June until mid-July, when it changed position and orientation, perhaps as a response to a **poleward** acceleration of the undercurrent over the slope; by early August the core of the jet lay about 150 km offshore at both Point Arena and Point Reyes. The intensity of the equatorward jet decreased, and the width of
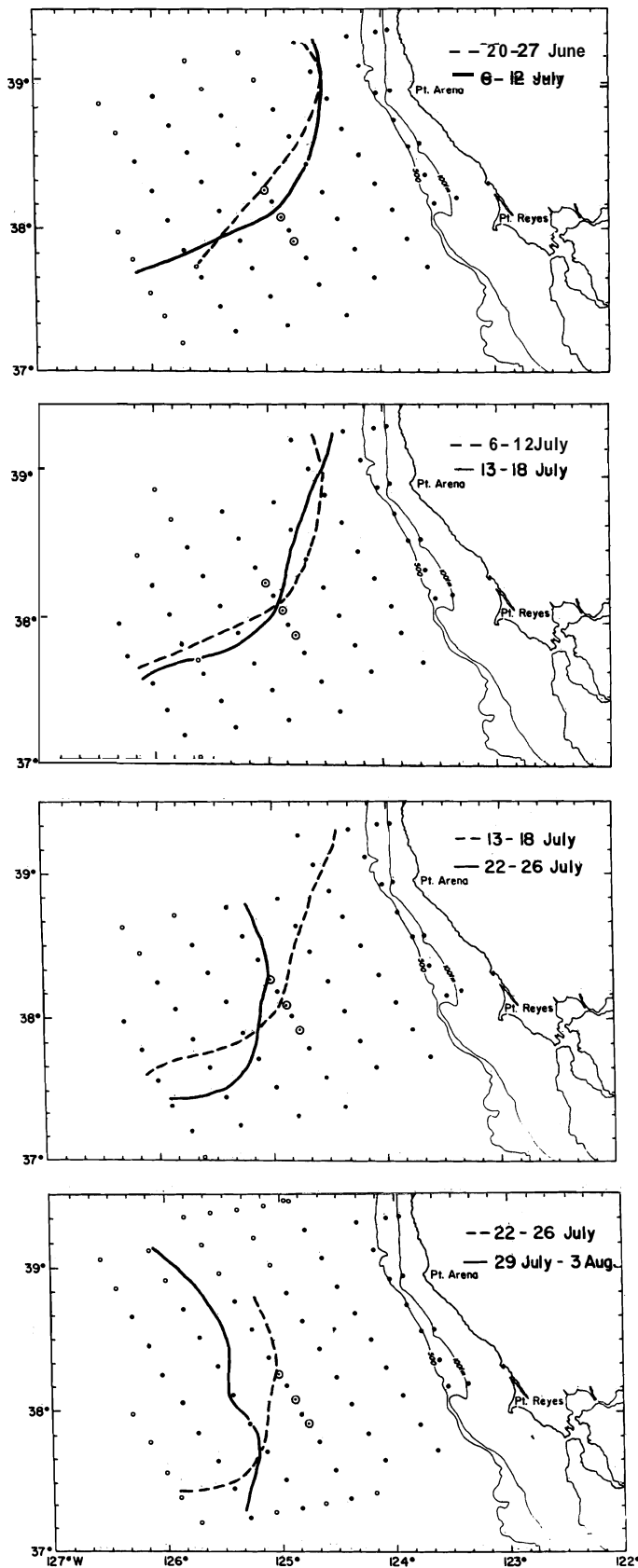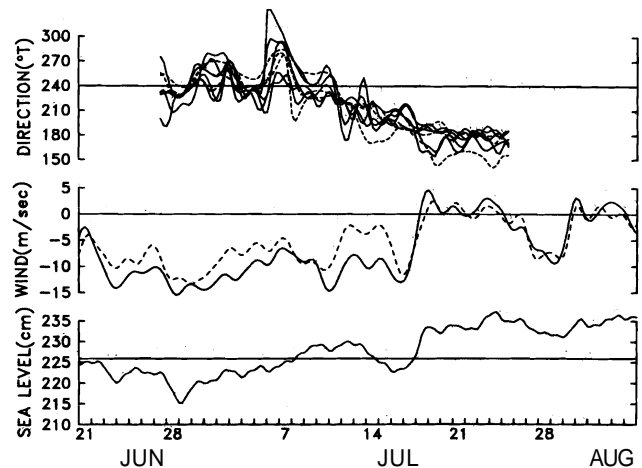
Fig. 21. Direction of low-pass-filtered velocity vectors at 20 and 88 m (solid lines) and near 200 m (dashed lines) from current meter moorings, alongshore component of wind vectors near Point Arena (dashed) and Bodega Bay (solid) shown in Figure 2, and low-pass-filtered sea level at Point Reyes.

the jet increased, during the 6-week sequence of surveys, while the baroclinic transport remained about the same (about **4** Sv relative to 500 dbar). The current meters moored across the axis of the jet at the beginning of the surveys remained in or adjacent to the jet throughout their deployment; the change in the jet's position in mid-July was, in effect, a rotation about the moorings. Prior to the rotation of the jet, the jet axis was nearly normal to the array, allowing an accurate estimate of the transport: The transport in the upper 500 m, estimated from the current meters, varied between **4** and 6 Sv with a mean of **4.8** Sv, in general agreement with the geostrophic estimate. Throughout the survey sequence and the mooring deployment period, the velocity in the jet decreased with depth by about a factor of 5 between the surface and **200** m; the jet was still discernible in the structure and variation of the deepest currents measured by the array ($>$ **400 m**) and in the lateral gradients of density, temperature, and salinity at **500** m. There is an absolute minimum in surface salinity near the axis of the jet, and in spite of patchiness, T-S characteristics along the axis were distinguishable from both inshore and offshore waters. It is possible, and even likely, that the equatorward jet observed in the CTZ region represents the core of the larger-scale California Current.

Inshore of the jet lay a poleward-flowing undercurrent whose baroclinic transport (relative to 500 dbar) increased from $<$0.5 Sv to $>$1.0 Sv between late June and early August **1988.** The core of this poleward flow lay adjacent to the continental slope at a depth of about 150–250 m; speeds of up to **20 cm s**$^{-1}$ were measured at **200** m. In this depth range the inshore waters were warmer and more saline than those offshore. The T-S characteristics were consistent with large-scale poleward advection and suggest that we observed a portion of the California Undercurrent.

We have provided an overview of the mesoscale structure of the currents and water masses observed in the coastal transiton zone in the summer of **1988.** Much more remains to be learned about the currents and water masses in the transition region, particularly on their formation, evolution

Fig. 20. The axis of the **equatorward** jet, marked by the 9.0 m^2 s^{-2} contour of the geopotential anomaly of the sea surface relative to 500 dbar. Each panel shows the jet axis in consecutive surveys, the current meter mooring positions (open circles), and CTD stations occupied during one or both surveys (open or solid dots, respectively).

and decay, and their relation to the California Current system as a whole.

REFERENCES

Brink, K. H., R. C. Beardsley, P. P. Niiler, M. Abbott, A. Huyer, S. Ramp, T. Stanton, and D. Stuart, Statistical properties of near-surface flow in the California coastal transition zone, *J. Geophys. Res.,* this issue.

Chavez, F. P., R. T. Barber, A. Huyer, P. M. Kosro, S. R. Ramp, T. P. Stanton, and B. Rojas de Mendiola, Horizontal transport and the distribution of nutrients in surface waters in the coastal transition zone off northern California: Effects on primary production, phytoplankton biomass, and species composition, *J. Geophys. Res.,* this issue.

Chelton, D. B., Seasonal variability of alongshore geostrophic velocity off central California, *J. Geophys. Res., 89,* 3473–3486, 1984.

Chereskin, T. K., E. Firing, and J. A. Gast, Identifying and screening filter skew and noise bias in acoustic Doppler current profiler measurements, *J. Atmos. Oceanic Technol., 6,* 1040–1054, 1989.

Coastal Transition Zone (CTZ) Group, The Coastal Transition Zone Program, *Eos Trans. AGU, 69,* 698–699, 704, 1988.

Davis, R. E., Drifter observations of coastal surface currents during CODE: The method and descriptive view, *J. Geophys. Res., 90,* 47414755, 1985.

Flament, P., Finestructure and subduction associated with upwelling filaments, Ph.D. dissertation, 142 pp., Univ. of Calif., San Diego, 1986.

Flament, P., L. Armi, and L. Washburn, The evolving structure of an upwelling filament, *J. Geophys Res., 90,* 11,765–11,778, 1985.

Fleischbein, J., R. E. Schramm, A. Huyer, P. M. Kosro, T. Cowles, and K. Krefft, CTD observations in the coastal transition zone off northern California, 18–27 June 1988, *Data Rep. 143, Ref. 88-9,* Coll. of Oceanogr. Oreg. State Univ., Corvallis, 1988.

Hayward, T. L., and A. W. Mantyla, Physical and biological structure of a coastal eddy near Cape Mendocino, *J. Mar. Res., 48,* d25-850, 1990.

Hickey, B. M., The California Current system—Hypotheses and facts, *Prog. Oceanogr., 8,* 191–279, 1979.

Hood, R. R., M. R. Abbott, A. Huyer, and P. M. Kosro, Surface patterns in temperature, flow, phytoplankton biomass, and species composition in the coastal transition zone off northern California, *J. Geophys. Res., 95,* 18,081–18,094, 1990.

Huyer, A., Coastal upwelling in the California Current system, *Prog. Oceanogr., 12,* 259–284, 1983.

Huyer, A., Hydrographic observations along the CODE Central line off northern California, **1981,** J. Phys. Oceanogr., *14,* 1647–1658, 1984.

Huyer, A., and P. M. Kosro, Mesocale surveys over the shelf and slope in the upwelling region near Point Arena, California, *J. Geophys. Res., 92,* 1655–1681, 1987.

Huyer, A., and R. L. Smith, A subsurface ribbon of cool water over the continental shelf off Oregon, *J. Phys. Oceanogr., 4,* 381–391, 1974.

Huyer, A., E. J. C. Sobey, and R. L. Smith, The spring transition in currents over the Oregon continental shelf, *J. Geophys. Res., 84,* 6995–7011, 1979.

Huyer, A., P. M. Kosro, S. Lentz, and R. C. Beardsley, Poleward flow in the California Current system, in *Poleward Flows Along Eastern Ocean Boundaries, Coastal Estuar. Studies,* vol. 34, edited by S. Neshyba, C. N. K. Mooers, R. L. Smith, and R. T. Barber, pp. 142–156, Springer-Verlag, New York, 1989.

Ikeda, M., and W. J. Emery, Satellite observations and modeling of meanders in the California Current system off Oregon and northern California, *J. Phys. Oceanogr., 14,* 1434–1450, 1984.

Kosro, P. M., Shipboard acoustic current profiling during the Coastal Ocean Dynamics Experiment, Ph.D. thesis, *SIO Ref. 85–8,* 119 pp., Scripps Inst. of Oceanogr., La Jolla, Calif., 1985.

Kosro, P. M., Structure of the coastal current field off northern California during the Coastal Ocean Dynamics Experiment, *J. Geophys. Res., 92,* 1655–1681, 1987.

Kosro, P. M., and A. Huyer, CTD and velocity surveys of seaward jets off northern California, July 1981 and 1982, *J. Geophys. Res., 91,* 7680–7690, 1986.

Kosro, P. M., A. Huyer, and R. L. Smith, Preliminary CTD/ADCP results of Wecoma cruise W8807A, *Coastal Transition Zone Newsl. 3(3),* pp. 2–8, Woods Hole Oceanogr. Inst., Woods Hole, Mass., 1988.

Kosro, P. M., A. Huyer, S. R. Ramp, R. L. Smith, F. P. Chavez, T. J. Cowles, M. R. Abbott, P. T. Strub, R. T. Barber, P. Jessen, and L. F. Small, The structure of the transition zone between coastal waters and the open ocean off northern California, winter and spring 1987, *J. Geophys. Res.,* this issue.

Lentz, S. J., and D. C. Chapman, Seasonal differences in the current and temperature variability over the northern California shelf during the Coastal Ocean Dynamics Experiment, *J. Geophys. Res., 94,* 12,571–12,592, 1989.

Lynn, R. J., and J. J. Simpson, The California Current system: The seasonal variability of physical characteristics, *J. Geophys. Res., 92,* 12,947–12,966, 1987.

Lynn, R. J., and J. J. Simpson, The flow of the undercurrent over the continental borderland off southern California, *J. Geophys. Res., 95,* 12,995–13,008, 1990.

Magnell, B. A., J. F. Borchardt, J. B. Andrews, J. M. Federiuk, E. D. Kinsella, and C. D. Winant, Northern California Coastal Circulation Study, Data report 2, Main measurement program, March–August 1988, vol 2, Moored instrument, meteorological and sea level observations, *Rep. NCCCS-89-17,* Miner. Manage. Serv., Los Angeles, Calif., 1990.

McDougall, T. J., Neutral surfaces, *J. Phys. Oceanogr., 17,* 1950–1964, 1987.

Mooers, C. N. K., Workshop summary: Poleward flow—observational and theoretical issues, in: *Poleward Flows Along Eastern Ocean Boundaries, Coastal Estuarine Stud.,* vol. 34, edited by S. Neshyba, C. N. K. Mooers, R. L. Smith, and R. T. Barber, pp. 2–16, Springer-Verlag, New York, 1989.

Mooers, C. N. K., C. A. Collins, and R. L. Smith, The dynamic structure of the frontal zone in the coastal upwelling region off Oregon, *J. Phys. Oceanogr., 6,* 3–21, 1976.

Moum, J. N., D. R. Caldwell, and P. J. Stabeno, Mixing and intrusions in a rotating cold-core feature off Cape Blanco, Oregon, *J. Phys. Oceanogr., 18,* 823–833, 1988.

Munk, W., Internal waves and small-scale processes, in *Evolution of Physical Oceanography,* edited by B. A. Warren and C. Wunsch, pp. 264-291, MIT Press, Cambridge, Mass., 1981.

Nelson, C. S., and D. M. Husby, Climatology of surface heat fluxes over the Caifornia Current region, *NOAA Tech. Rep., NMFS SSRF-763,* 155 pp., 1983.

Paduan, J. D., and P. P. Niiler, A Lagrangian description of motion in northern California coastal transition filaments, *J. Geophys. Res., 95,* 18,095–18,109, 1990.

Ramp, S. R., P. F. Jessen, K. H. Brink, P. P. Niiler, F. L. Daggett, and J. S. Best, The physical structure of cold filaments near Point Arena, California, during June 1987, *J. Geophys. Res.,* this issue.

Reid, J. L., Intermediate waters of the Pacific Ocean, *Johns Hopkins Oceanogr. Stud., 2,* 85 pp., 1965.

Reid, J. L., G. I. Roden, and J. G. Wyllie, Studies of the California Current system, report, July 1, 1956–January 1958, pp. 28–56, *Calif. Coop. Oceanic Fish. Invest.,* La Jolla, Calif., 1958.

Rienecker, M. M., and C. N. K. Mooers, Mesoscale eddies, jets, and fronts off Point Arena, July 1986, *J. Geophys. Res., 94,* 12,555–12,569, 1989.

Rienecker, M. M., C. N. K. Mooers, D. E. Hagan, and A. R. Robinson, A cool anomaly off northern California: An investigation using IR imagery and in situ data, *J. Geophys. Res., 90,* 48074818, 1985.

Robinson, M. K., Atlas of North Pacific Ocean monthly mean

temperatures and mean salinities of the surface layer, *Ref. Publ. 2,* Nav. Oceanogr. Off., Washington, D. C., **1976.**

Strub, P. T., et al., The nature of the cold filaments in the California Current system, J. *Geophys. Res.,* this issue.

Thomson, R. E., and J. E. Papadakis, Motion of satellite-tracked drifter along the west coast of North America, J. *Geophys. Res., 92,* 6445–6461, **1987.**

Tibby, R. B., The water masses off the west coast of North America, J. *Mar. Res., 4,* **112–121, 1941.**

Tully, J. P., and F. G. Barber, An estuarine analogy in the sub-Arctic Pacific Ocean, J. *Fish. Res. Board Can., 17,* **91–112, 1960.**

Veronis, G., On the properties of seawater defined by temperature, salinity, and pressure, J. *Mar. Res., 30,* **227–255, 1972.**

Winant, C. D., R. C. Beardsley, and R. E. Davis, Moored wind, temperature and current observations made during Coastal Ocean Dynamics Experiments 1 and **2** over the northern California continental shelf and upper slope, J. *Geophys. Res., 92,* 1569–**1604, 1987.**

Wooster, W. S., and J. L. Reid, Eastern boundary currents, in *The Sea,* vol. **2,** edited by M. N. Hill, pp. **253–280,** Interscience, New York, **1963.**

Wyrtki, K., The dynamic topography of the Pacific Ocean and its fluctuations, *Rep. HZG-74-5,* Hawaii Inst. of Geophys., Univ. of Hawaii, Honolulu, **1974.**

_____

F. P. Chavez, Monterey Bay Aquarium Research Institute, **160** Central Avenue, Pacific Grove, CA **93950.**

T. J. Cowles, J. Fleischbein, A. Huyer, P. M. Kosro, S. D. Pierce, and R. L. Smith, College of Oceanography, Oregon State University, Corvallis, OR **97331.**

S. R. Ramp and T. Stanton, Department of Oceanography, Naval Postgraduate School, Monterey, CA **93943.**

L. Washburn, Department of Geography, University of California, Santa Barbara, Santa Barbara, CA **93106.**